Powder Technology 469 (2026) 121854

Contents lists available at ScienceDirect

Powder Technology

journal homepage: www.journals.elsevier.com/powder-technology

Influence of particle morphology and solvent choice on the sublimation of recrystallised ibuprofen at ambient pressure and sub-melting temperatures

Ameer Alshukri [a], Sven L.M. Schroeder [a,b,c], Ana Kwokal [d], Ali Hassanpour [a,*]

[a] School of Chemical and Process Engineering, University of Leeds, Leeds LS2 9JT, UK
[b] Diamond Light Source, Chilton, Didcot OX11 0DE, UK
[c] Continuous Manufacturing and Advanced Crystallisation (CMAC) Group, Research Complex at Harwell, Chilton, Didcot OX11 0FA, UK
[d] Syngenta, Jealott's Hill, Warfield, Bracknell RG42 6EY, UK

HIGHLIGHTS

- Ibuprofen sublimes below its melting point at ambient pressure.
- Solvent choice controls crystal morphology and sublimation kinetics.
- Normalised rates reveal facet-dependent sublimation; polar-facet accelerates mass loss.

GRAPHICAL ABSTRACT

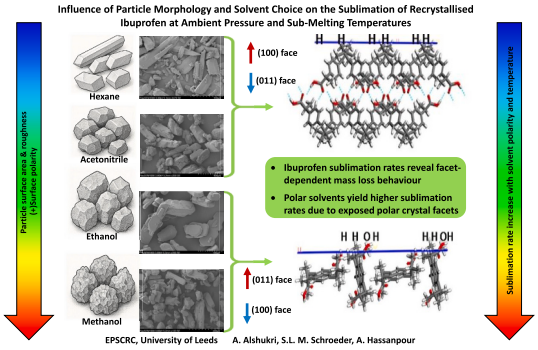

ARTICLE INFO

Keywords:
Ibuprofen sublimation
Particle morphology
Crystallisation solvents
Surface energy
Thermal analysis (TGA, DVS)
Pharmaceutical stability

ABSTRACT

The tendency of ibuprofen to sublimate can undermine content uniformity and cause caking during storage, resulting in significant economic losses. While previous studies have predominantly investigated typical evaporation under vacuum, the solvent-mediated relationship between crystal structure, sublimation kinetics and thermodynamics under practical conditions remains unclear. This study aimed to determine how crystallisation solvent governs ibuprofen sublimation under ambient pressure and sub-melting temperatures, independent of particle size, by linking crystal structure and morphology to sublimation behaviour. Ibuprofen was recrystallised from hexane, acetonitrile, ethanol and methanol, with composition and structure verified using FTIR and PXRD. SEM and particle size analysis quantified morphology and surface area, while sublimation kinetics were measured by TGA and DVS under storage-relevant conditions and subsequently enthalpy of sublimation and change in vapour pressure by temperature were estimated. It was found that polar-solvent crystals have higher surface energy and faster sublimation, while non-polar-solvent crystals were more stable and slower sublimation. The obtained enthalpy of sublimation was lower for polar-solvent samples and estimated change in vapour pressure by temperature aligned with literature trends. Overall, crystallisation solvent is a critical determinant of ibuprofen sublimation under storage-relevant conditions, influencing plane orientation, crystallinity and morphology. Polar solvents promote faster dissolution and potentially enhanced therapeutic performance but

* Corresponding author.
E-mail address: A.Hassanpour@leeds.ac.uk (A. Hassanpour).

https://doi.org/10.1016/j.powtec.2025.121854
Received 15 August 2025; Received in revised form 28 October 2025; Accepted 31 October 2025
Available online 1 November 2025

increase sublimation risk, whereas non-polar solvents improve storage stability at the expense of dissolution rate. These findings provide practical guidance for optimising solvent selection to balance pharmaceutical performance, stability and manufacturing efficiency.

1. Introduction

Ibuprofen is a widely used nonsteroidal anti-inflammatory drug (NSAID) indicated for the treatment of inflammation, pain and fever [1]. Given its ubiquitous use, global production of ibuprofen powder exceeds 5000 metric tons per year, approximately 10 % of global active pharmaceutical ingredient (API) demand [2]. The physical characteristics of pharmaceutical powders such as thermal stability, polymorphic form, flowability, compressibility, dissolution behaviour and particle size and shape play crucial roles in manufacturing and processing. These properties directly influence medicine production processes such as the tableting, by significantly affecting dosage uniformity and the consequent therapeutic efficacy [3]. Powder flowability, agglomeration, and uneven component distribution can lead to segregation and lump formation, hindering flow and dosing and causing variability in tablet weight and content uniformity [4]. Understanding and controlling these parameters are essential for the handling and manufacturability of pharmaceutical powders.

Ibuprofen is a white crystalline powder with the molecular formula $C_{13}H_{18}O_2$, a molecular weight of 206.27 g/mol and a melting point of 75–77 °C [5]. The molecule contains a chiral carbon at the α-position adjacent to the carboxyl group. Commercial ibuprofen is typically the racemate, RS-(±)-ibuprofen, comprising the enantiomers S-(+)-ibuprofen and R-(−)-ibuprofen. The pure S-enantiomer exhibits higher pharmacological efficacy than the racemate [6]; it also has a significantly lower melting point, greater solubility, a higher dissolution rate and a different crystal structure [7].

The thermal properties of ibuprofen were first documented in 1990. Differential scanning calorimetry (DSC) showed that both the degree of crystallinity and the crystallisation solvent influence the material's melting point [8]. Standard melting-point measurements further demonstrated that ibuprofen crystallised from media such as glycerine, diethylene glycol, propylene glycol and polyethylene glycol (PEG) 3000 or 4000 exhibits melting-point variation attributable to differences in crystal habit [9]. Romero et al. proposed that the stereochemical configuration of ibuprofen affects its crystal structure and physical properties; specifically, (+)-ibuprofen displayed a lower melting point than the racemate [10,11]. Consistent with these observations, Dwivedi et al. reported that the (+) and (−) isomers melt at 46–54 °C, markedly below the racemate's 76–78 °C [12].

Lerdkanchanaporn and Dollimore [13] evaluated the thermal stability of ibuprofen under isothermal conditions. They reported that ibuprofen volatilises between its melting and boiling points, with a surface-controlled evaporation process. The evaporation activation energy (E_a) was estimated at ≈81.8–87.0 kJ/mol which is approximately double the enthalpy of vaporisation (ΔH_vap) predicted via Trouton's rule. This discrepancy suggests that ibuprofen forms dimers in the liquid state that dissociate into monomers in the vapour phase.

Xu et al. [14] addressed gaps in existing data by using adiabatic calorimetry to obtain precise heat-capacity measurements, identify phase transitions and derive thermodynamic functions, thereby clarifying the thermal properties and evaporation kinetics of ibuprofen. They reported a melting point of 74.87 °C and an evaporation activation energy of 80.3 ± 1.4 kJ/mol. Evaporation begins at approximately 186.85 °C, with the maximum rate observed at 254.85 °C. The process follows zero-order kinetics, as evidenced by linear mass-loss rates, which is consistent with previous studies. The high activation energy helps explain ibuprofen's stability under typical storage conditions, while also highlighting risks at elevated temperatures.

Later, Tita et al. [15,16] examined the thermal degradation and stability of ibuprofen under both non-isothermal and isothermal conditions, using methodologies that adhered to modern standards (ICTAC protocol, 2000) to address limitations of earlier single-rate studies. DSC confirmed a melting point consistent with literature values (75–78 °C), with complete melting at ≈79 °C. Although increasing heating rates shifted thermal curves to higher temperatures, the melting process itself was largely unaffected. Melting was followed by decomposition, with subsequent evaporation of volatile products. Decomposition occurred between 180 and 300 °C, with a peak temperature (T_max) of ≈282 °C, ending in complete mass loss and proceeded as a single, well-defined step. B. Tiţa et al. further analysed the kinetic parameters of ibuprofen's thermal decomposition and established a first-order mechanism, determining E_a, reaction order (n), and pre-exponential factor (A). Kinetic parameters derived under isothermal and non-isothermal conditions were consistent.

Sublimation is a fundamental thermodynamic phase transition in which a solid converts directly to a gas without passing through the liquid state. The process is governed by temperature and pressure and typically occurs below a substance's triple point (the unique condition at which solid, liquid, and gas phases coexist). Sublimation is generally endothermic, requiring sufficient energy to overcome intermolecular forces within the solid lattice. The enthalpy of sublimation is the energy required to transform one mole of a substance directly from the solid to the gaseous phase at constant temperature and pressure. Sublimation can be quantified by various methods with different considerations. Vapour-pressure techniques (Knudsen/torsion effusion, transpiration) provide equilibrium pressures and, via Clausius–Clapeyron relation, robust sublimation enthalpy can be determined. This is excellent for moderately volatile, thermally stable solids but they require true equilibrium and leak-free setups [17,18]. Calorimetry (DSC, isothermal calorimetry) measures heat flow directly and yields sublimation enthalpy without absolute pressures, but can conflict sublimation with concurrent processes (softening, polymorphic transitions) unless baselines and reference are rigorously controlled [19]. Mass-loss approaches, such as thermogravimetric analysis (TGA), quartz crystal microbalance (QCM) and temperature-programmed desorption, offer sensitive rates and kinetics but may be transport-limited and often need calibration to relate rates to absolute vapour pressures [20]. Molecular-beam and mass-spectrometric effusion add species selectivity, resolving stoichiometry and decomposition products, at the cost of more complex instrumentation [21]. In practice, vapour-pressure/effusion methods are preferred for equilibrium sublimation enthalpy; calorimetry offers a direct energetic cross-check; and TGA/QCM methods are ideal for studying rate laws, activation energies and materials where surfaces, morphology or impurities strongly modulate sublimation. Careful control of temperature gradients, surface area and sample history (polymorph, crystal size, residual solvent) is critical across all methods to avoid kinetic artefacts masked as thermodynamics.

Freeze-drying (lyophilisation) during primary drying is controlled by coupled processes(heat and mass transfer) as the sublimation front moves through the porous cake and vapour escapes to the chamber. Classical, conduction-limited models with constant properties often under-predict drying rates and overlook practical constraints. Chaurasiya et al. instead used conduction–convection models that resolve vapour flow and evolving thermal behaviour, giving more accurate process-kinetics predictions and a robust sublimation-limit curve that defines a safe operating window [22–25,26]. The work shows that gas-phase convection and temperature-dependent transport properties can substantially speed up lyophilisation when combined with targeted internal heating, provided pressure limits are respected. Conversely, a

higher vapour heat capacity introduces thermal inertia that slows the sublimation front, while increased permeability within the samples at higher temperatures eases vapour removal and shifts mass-transfer resistance. Boundary heat losses and vial-edge effects further modulate drying rates.

The vapour pressure of ibuprofen was first reported by Ertel et al. [27] using the Knudsen effusion method to derive the enthalpy of sublimation for the racemate. Later, Perlovich et al. [28] employed the transpiration method to measure the vapour pressures of S-ibuprofen and the racemate and to calculate their sublimation enthalpies. The racemate exhibits a higher enthalpy of sublimation (115.8 kJ/mol) than the S-enantiomer (107.4 kJ/mol), indicating stronger intermolecular interactions and greater solid-state stability consistent with more efficient packing and hydrogen-bonding symmetry. Entropy plays only a minor role in the sublimation process as the process was mainly (62 %) enthalpy-driven for both forms. However, there is a small difference of 5 (kJ/mol) in the sublimation enthalpy for the racemate compound from both studies. Bellec and Guillemin [29] exploited the difference in vapour pressures between S-ibuprofen and the racemate to purify enantiomerically enriched samples. Sublimation was performed at 35–45 °C under reduced pressure (0.1 mbar) for ≈16 h, during which the mass change was ≈5–10 mg (≈0.5–1 %). Starting from a solid with a low initial enantiomeric excess (ee) of ≈10 %, sublimation yielded a sublimate with an ee near 85 %. These results indicate that sublimation can be an efficient method for isolating a high-purity single enantiomer when carried out at sub-melting temperatures and reduced pressure.

More recently Lin et al. [30], took advantage of ibuprofen's tendency to sublime under mild conditions prepare ibuprofen–nicotinamide cocrystals via vapour-phase crystallisation. Ibuprofen was sublimed at 65 °C under low pressure (10 Pa). The study identified 65 °C as the optimal sublimation temperature: powder X-ray diffraction (PXRD) and Fourier-transform infrared spectroscopy (FTIR) showed that above this temperature the ibuprofen crystal lattice begins to disrupt and substantially higher temperatures risk thermal decomposition. Accordingly, a sublimation temperature of 65 °C provides efficient vapour production without compromising crystal integrity. By contrast, unintended sublimation in large-scale powder manufacturing can cause a myriad of quality issues and significant economic losses by introducing variability into the process. Temperature and pressure strongly influence sublimation kinetics. When these parameters are not tightly controlled at scale, variable sublimation rates can arise, leading to batch-to-batch variability and potential quality defects [31].

As ibuprofen has low melting point (≈75 °C) its more susceptibility to sublimation under thermal-stress environment (e.g. in hot-melt extrusion) meaning even minor sublimation at elevated temperatures reduces yield making it a critical economic concern in large-scale production [32]. The design of equipment is also important because large-scale systems may struggle to maintain a uniform control over pressure and temperature, exacerbating the sublimation risks compared to lab-scale setups [33].

Sublimation can also alter the physicochemical properties of an API, including dissolution rate, flowability, and compressibility. These properties are critical for consistent drug performance and manufacturability. For example, sublimation-induced changes in particle size and density can impair powder flow during tablet manufacture, leading to process inconsistency and making batch-to-batch uniformity difficult to maintain [31,34,35]. The main issue caused by sublimation is the unintended loss of the active ingredient, resulting in reduced potency and potential non-compliance with dosage specifications. To mitigate this, formulations may incorporate substances such as glycol, glycerol, or copovidone to suppress sublimation and preserve the API within the solid preparation [36]. Ertel et al. [27] reported that the vapour pressure of ibuprofen is sufficiently high that powder stored in glass vials at 40 °C developed turbidity on the inner surface of the glass, consistent with sublimation. Practically, sublimation behaviour across a wide temperature range is of pharmaceutical interest for both physical and chemical stability, given the different temperatures used during drying and storage.

TGA and dynamic vapour sorption (DVS) are commonly used analytical techniques to evaluate material behaviour under different conditions and physicochemical differences between crystal forms [37,38,39,40]. TGA is used to measure the mass change of a sample as it is heated or cooled under controlled conditions, thereby providing insight into thermal stability and composition.Gückel et al. [41] measured sublimation rates of pesticides at ambient pressure by isothermal thermogravimetry, exploiting a linear relationship between log (sublimation rate) and log (vapour pressure) at a given temperature. Under isothermal conditions, the rate of mass loss due to vaporisation should be constant if both processes are zero-order. Subsequent studies have likewise used TGA to estimate vapour pressure and to investigate solid-state thermal degradation of pharmaceutical compounds, often observing linear mass-loss profiles characteristic of sublimation [42,43,44,45]. More recently Ruz et al. [46], used isothermal TGA to determine the enthalpy of sublimation and vapour pressure of 2-(2-nitrovinyl)furan (G-0), demonstrating the technique's effectiveness for extracting thermodynamic properties. In another study, the thermal decomposition and sublimation behaviour of TATB were investigated using a combined TGA/DSC instrument. The effects of confinement, starting mass and heating rate on TATB's thermal behaviour were examined, providing valuable insight into the kinetics of sublimation and decomposition [47].

By contrast, DVS is primarily designed to assess vapour sorption in materials (e.g. pharmaceuticals, foods and polymers). The vapour concentration around a sample is controlled, and the corresponding mass change is recorded. This approach can detect subtle transitions, such as amorphous-to-crystalline conversion [48]. However, DVS can also be utilised to probe the influence of moisture on sublimation behaviour, as the literature on the effect of humidity on sublimation kinetics in pharmaceutical solids remains sparse.

Crystallisation is used to engineer ibuprofen particles to achieve desirable physicochemical and biopharmaceutical properties and to improve manufacturing and handling behaviour [49,50]. This is typically accomplished by adjusting key process parameters during crystallisation, which directly influence particle size, morphology, and polymorphism. Among these parameters, solvent selection plays a critical role because it governs crystal nucleation, growth kinetics, and polymorphic outcome. Variations in these factors can lead to significant differences in solid-state properties that are critical for product handling, production efficiency, and therapeutic performance [9,51,52].

Although numerous studies have examined ibuprofen's thermal properties, decomposition kinetics, enthalpy of sublimation and the effects of crystallisation on pharmaceutical performance, the role of particle morphology and the influence of crystallisation-solvent polarity on ibuprofen's sublimation behaviour at sub-melting temperatures remains unexplored. The aim of this study is to quantify the sublimation rate of ibuprofen at ambient pressure and at temperatures below its melting point, replicating real-world storage and handling conditions. Ibuprofen samples recrystallised from four different solvents were characterised for crystallinity (PXRD), molecular structure (FTIR), particle size (optical microscopy), morphology (scanning electron microscopy) and sublimation rate (TGA and DVS) under ambient conditions.

2. Experimental

Grade 50 racemic (RS) ibuprofen powder was obtained from BASF (UK). Organic solvents used for recrystallisation included hexane (Hex) and acetonitrile (MeCN) (both >99 %; Sigma-Aldrich, UK), and ethanol (EtOH) and methanol (MeOH) (both >99.8 %; VWR Chemicals, UK).

A cooling recrystallisation method was used. For each solvent, 54 g of ibuprofen powder was placed in a 100 mL AutoMATE reactor vessel (H.E.L. Group, UK) and 25 mL of the chosen solvent was added. The

mixture was then heated to the minimum temperature required to achieve complete dissolution. For the polar solvents (MeOH and EtOH), a reactor temperature of 50 °C was sufficient to obtain a homogeneous solution. For the less polar solvents (MeCN and Hex), the temperature was increased to 60 °C to overcome lower solubility and ensure full dissolution [50,53]. Once a clear solution was obtained, the mixture was cooled at 1 °C/min to 36 °C and the reactor was seeded with 1 % of the starting material. The solution was then held at 36 °C for 30 min to promote nucleation, followed by further cooling to 0 °C over 120 min. The resulting slurry was stirred at 0 °C for an additional 120 min to ensure complete crystallisation. The slurry was filtered through a general-purpose laboratory Büchner funnel (VWR Chemicals, UK) with Grade 1 filter paper (Whatman, UK). The isolated white solid was dried in a vacuum oven at 40 °C for 24 h. (See Fig. 1 for Schematic workflow)

Following drying, each recrystallised batch was examined by attenuated total reflectance–Fourier-transform infrared (ATR-FTIR) spectroscopy to confirm molecular structure and sample purity. A Thermo Fisher Scientific IS 10 instrument equipped with a diamond crystal and a Smart iTR ATR module was used. Each spectrum was acquired as the average of 32 interferograms after the samples were subjected to ≈10,000 psi using a high-pressure clamp. Qualitative analysis was performed over 600–4000 cm^{-1}, with background absorption subtracted from the sample spectra.

A series of 200-mm diameter stainless-steel sieves (Endecotts Ltd., UK) with aperture sizes ranging from 53 μm to 450 μm was used to isolate each batch into separate sample sieve cut. A maximum of 20 g of powder was used to ensure adequate agitation and particle reorientation without clogging the sieve and to reproducible separations. Sieving was conducted using a sieve shaker (EML, Haver & Boecker, Germany), operating at an amplitude of 1.3 mm for a duration of 120 min. To prevent particle breakage, parameters were selected in line with sieve-analysis guide by (Retsch GmbH, Germany) and preliminary tests following DIN 66165 standard, which deems sieving complete when mass change is <0.1 % over one minute. An amplitude of 1.3 mm was employed to achieve statistical resonance where particles optimally reorient and pass through the mesh with each lift by synchronising throw time with the sieve-bottom vibration period.

To qualitatively evaluate particle size, shape, and surface topography, scanning electron microscopy (SEM) was performed using a Hitachi FlexSEM 1000 II instrument. The SEM operated at 3 kV with a working distance of ≈5 mm. Samples were first mounted on carbon-adhesive tabs affixed to metal pin stubs, then sputter-coated with a ≈ 5 nm silver layer using a K575X Emitech Quorum sputter coater to reduce charging during imaging.

An Empyrean diffractometer (Malvern Panalytical Ltd., UK) was used to collect powder diffraction patterns. A standard Empyrean powder holder was used in Bragg–Brentano geometry. The X-ray source operated at 45 kV and 40 mA to generate Cu Kα radiation (λ = 0.154 nm). Scans were performed over 2θ = 4–40° with a step size of 0.0167°. For each sample, the area under the curve (AUC) for the (011) and (100) reflections was computed and expressed as a fraction of the total integrated intensity across all PXRD peaks. The AUC ratio (011):(100) was also calculated to compare the relative contributions of these facets.

Particles from each sieve fraction for both as-received ibuprofen and solvent-recrystallised samples were characterised using a Morphologi G3-S (Malvern Instruments Ltd., UK). Particle-size distribution (PSD), shape and projected area were measured. A dry powder volume of 7 mm^3 was dispersed via the instrument's sample-dispersion unit using nitrogen at 1 bar with a 20-millisecond injection. The dispersed sample was allowed to settle for 60 s on the G3 glass stage, after which a 5× objective (measurement range 6.5–420 μm) was used for image capture. The Morphologi G3 software was used to analyse particle metrics, with circle-equivalent diameter (CE diameter) reported for size and aspect ratio for shape.

To estimate the surface area of the particles, the CE diameter d was used to calculate the surface area and volume of a sphere for each particle captured by the G3 instrument during every run. A total of 45 runs were conducted across 15 different batches. The specific surface area A_s was then calculated according to eq. 1. Where ρ is the density of ibuprofen, which is 1.03 g/cm^3.

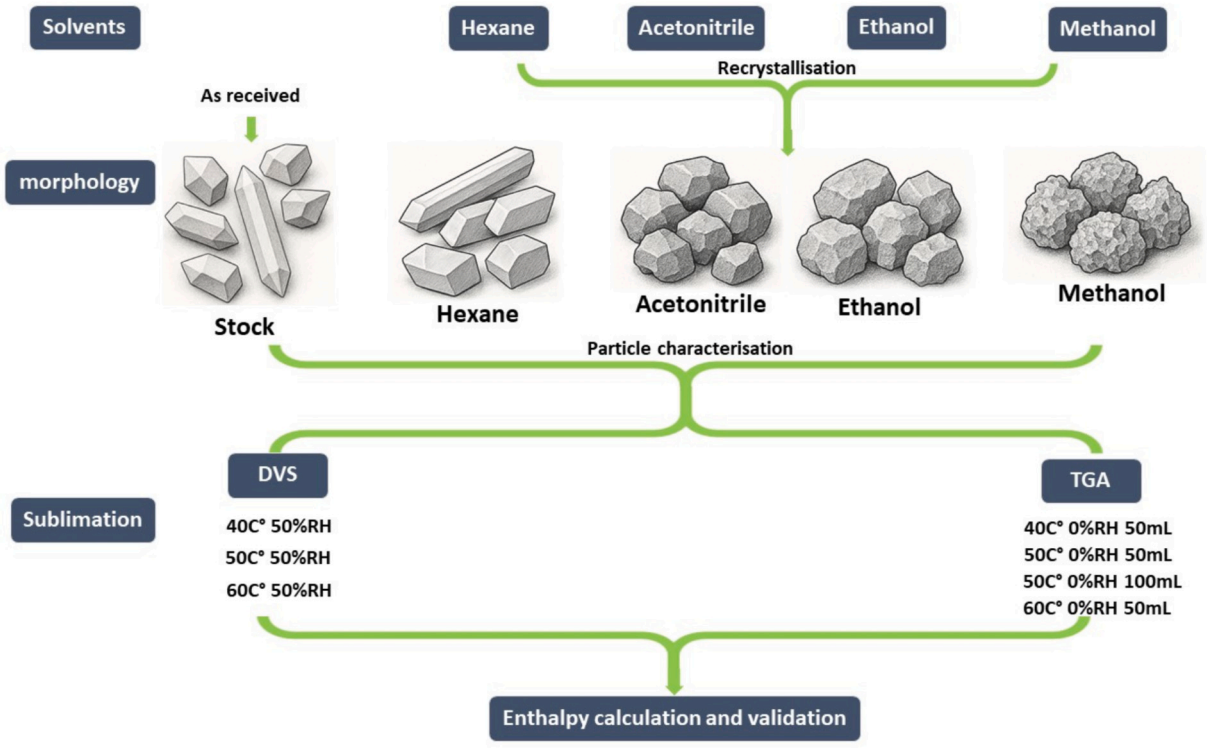

Fig. 1. Schematic illustrating the workflow from solvent selection and crystallisation to the resulting particle morphology followed by the sublimation parameters assessed.

The specific surface area is defined as the total surface area of all particles (in cm^2) divided by the total volume of all particles (in cm^3). Since the mass of each sample differs, the surface area per unit mass (cm^2/g) was calculated by dividing the surface area per unit volume (cm^{-1}) by the absolute density of ibuprofen (1.03 g/cm^3).

$$A_s = \frac{A}{\rho V} = \frac{6}{\rho d} \quad (1)$$

The rate of sublimation of ibuprofen powder was measured by TGA, leveraging the instrument's capability to continuously record sample mass under a precisely controlled temperature programme. Approximately 10 mg of powder was placed in a 100 μL platinum pan and loaded into a Discovery TGA 5500 (TA Instruments, USA). The temperature was ramped at 20 °C per minute to the target temperature. Three targets were investigated: 40, 50, and 60 °C. An isothermal hold of 320 min was maintained once the set temperature was reached. A constant nitrogen purge of 50 mL/min was used throughout. The effect of purge flow on sublimation rate was also assessed at 50 °C by increasing the flow to 100 mL/min.

DVS was used in two modes. First, a single relative-humidity (RH) cycle was applied, increasing humidity in 10 % RH steps up to 90 % RH and then returning to 0 % RH at 25 °C. An equilibrium criterion of 0.002 % (dm/dt) per step was used. Nitrogen at 400 sccm served as the carrier gas. This test assessed the hygroscopicity of ibuprofen. Second, the effect of humidity on sublimation rate at different temperatures was investigated. Experiments were conducted at 40, 50, and 60 °C, each at 50 % RH. Humid conditions were generated by mixing dry and water-saturated nitrogen, with a total flow of 400 sccm. The ultrabalance was calibrated whenever conditions changed by allowing the chamber to equilibrate to the target setpoint and following the instrument's calibration wizard. After calibration, ≈50 mg of powder was loaded into a 10 mm stainless-steel pan and analysed on a DVS Endeavour (Surface Measurement Systems Ltd., UK). The instrument's ultrabalance has a resolution of 0.01 μg and noise <0.3 μg, and can run up to five samples in parallel.

3. Results and discussion

3.1. FTIR and XRD

Ensuring a high degree of purity and structural integrity in ibuprofen is essential for reliable sublimation studies, so that any measured mass loss can be attributed to ibuprofen rather than impurities. FTIR spectroscopy of all solvent-recrystallised batches produced spectra identical to the commercial stock, indicating no chemical alteration (Supplementary Information, Fig. S1). XRD patterns revealed solvent-dependent differences in peak intensities and lattice parameters, reflecting variations in crystallite size, morphology and preferred orientation (Supplementary Information, Fig. S2). Specifically, recrystallisation from polar solvents (MeOH, EtOH) yielded well-defined, highly crystalline material with pronounced plane alignment, whereas non-polar (Hex) and semi-polar (MeCN) solvents produced more aggregated particles of reduced crystallinity and selective plane development. Crucially, across all solvent systems, the crystalline form, chemical purity and overall structural integrity of ibuprofen were preserved.

3.2. Scanning electron microscopy

SEM micrographs of the stock ibuprofen at 500, 400, and 100 μm are shown in Fig. 2a. The images reveal irregularly shaped crystals with pronounced heterogeneity in both size and morphology. Many crystals are elongated, prismatic, and uneven features likely arising from the use of a non-polar solvent during manufacture (hexane, per the manufacturer's specification) and from mechanical breakage during shipping and handling. Such elongated habit is typical of crystallisation from non-polar solvents like Hex. This lack of uniformity is characteristic of the unprocessed, as-received material.

Fig. 2b shows SEM micrographs of ibuprofen recrystallised from Hex. The particles are predominantly elongated, as expected when Hexpromotes growth along specific crystallographic axes, yielding a characteristic needle-like morphology. Many particles display high aspect ratios, consistent with anisotropic crystal growth. Compared with the as-received stock (also crystallised from Hex), the images indicate inconsistent outcomes, suggesting batch-to-batch variation. The sample does not exhibit the smoothness and uniformity typically associated with well-recrystallised material; instead, surfaces appear fragmented and coarse, which may indicate incomplete recrystallisation or suboptimal growth conditions.

SEM micrographs of the MeCN-recrystallised sample (Fig. 2c) show small, cuboid-like crystals with some clustering. Particle surfaces appear non-uniform, with satellite fragments attached to the primary crystals. In contrast, EtOH-recrystallised ibuprofen (Fig. 2d) exhibits block-like, aggregated crystals. Larger crystals tend to adhere to one another, whereas the stock material is more unevenly dispersed. The presence of smaller crystals in the form of agglomeration might be due to varying nucleation and growth during recrystallisation influenced by EtOH.

Fig. 2e shows SEM images of MeOH-recrystallised ibuprofen, which display clear morphological differences from the stock material: crystals are more block-like with distinct facets. A slight elongation is present, but the dominant habit remains cuboid-like. MeOH appears to promote growth inhibition along specific crystallographic directions, yielding a more equant morphology that favours flowability, packing, and batch-to-batch reproducibility, superior to the as-received powder for handling purposes. Mechanistically, MeOH may stabilise certain crystal faces via hydrogen-bonding interactions with the carboxyl (COOH) group, moderating solute–solvent interactions during growth.

3.3. G3 Morphologi

Volume-based particle parameters obtained using the G3 morphology method are summarised in Table 1. The equivalent circular diameter and the aspect ratio (the ratio of the shortest to the longest dimension) are key descriptors of particle size and shape. Elongated, needle-like particles have low aspect ratios, whereas near-circular particles have high aspect ratios (approaching 1).

Although the measured CE D_{50} values decrease as the sieve aperture decreases, there is a consistent discrepancy between D_{50} and the sieve-size ranges used during sieving. In many cases, the measured D_{50} underestimates the mean sieve aperture because sieves preferentially retain larger particles while fines pass through, skewing the retained fraction toward smaller sizes. For example: Hex_100–140, mean sieve aperture = 120 μm, D_{50} = 64 μm (Δ = −56 μm); MeCN_75–90, mean sieve aperture = 82.5 μm, D_{50} = 80 μm (Δ = −2.5 μm). This discrepancy is sample-dependent: coarser, more blocky material such as Hex_100–140 (aspect ratio = 0.50) exhibits a larger negative Δ, whereas more rounded/near-spherical particles such as MeCN_75–90 (aspect ratio = 0.60) show a Δ close to zero. Here, Δ is defined as D_{50} − mean sieve aperture (negative values indicate D_{50} < aperture).

The aspect ratio appears to play a big role as samples with higher aspect ratios (more round particles) exhibit a closer match between D_{50} and the mean sieve aperture e.g. MeCN samples (AR ≈ 0.60–0.61) with difference between (D_{50}– mean sieve aperture) spanning −2.5 to +7 μm. In contrast, Stock samples (AR ≈ 0.41–0.43) span −44.5 to −8.5 μm. This pattern supports the interpretation that rounded particles orient more uniformly during sieving, thereby yielding D_{50} values nearer the mean aperture, whereas plate-like or elongated particles skew the retained fraction toward finer sizes.

For most samples, the measured D_{10} lies below the nominal minimum sieve aperture, while D_{90} lies near or slightly above the nominal maximum aperture. This reflects that sieving mechanically excludes most oversize particles but can retain some fines via interlocking/bridging; shape effects, agglomeration, and aperture tolerances can also

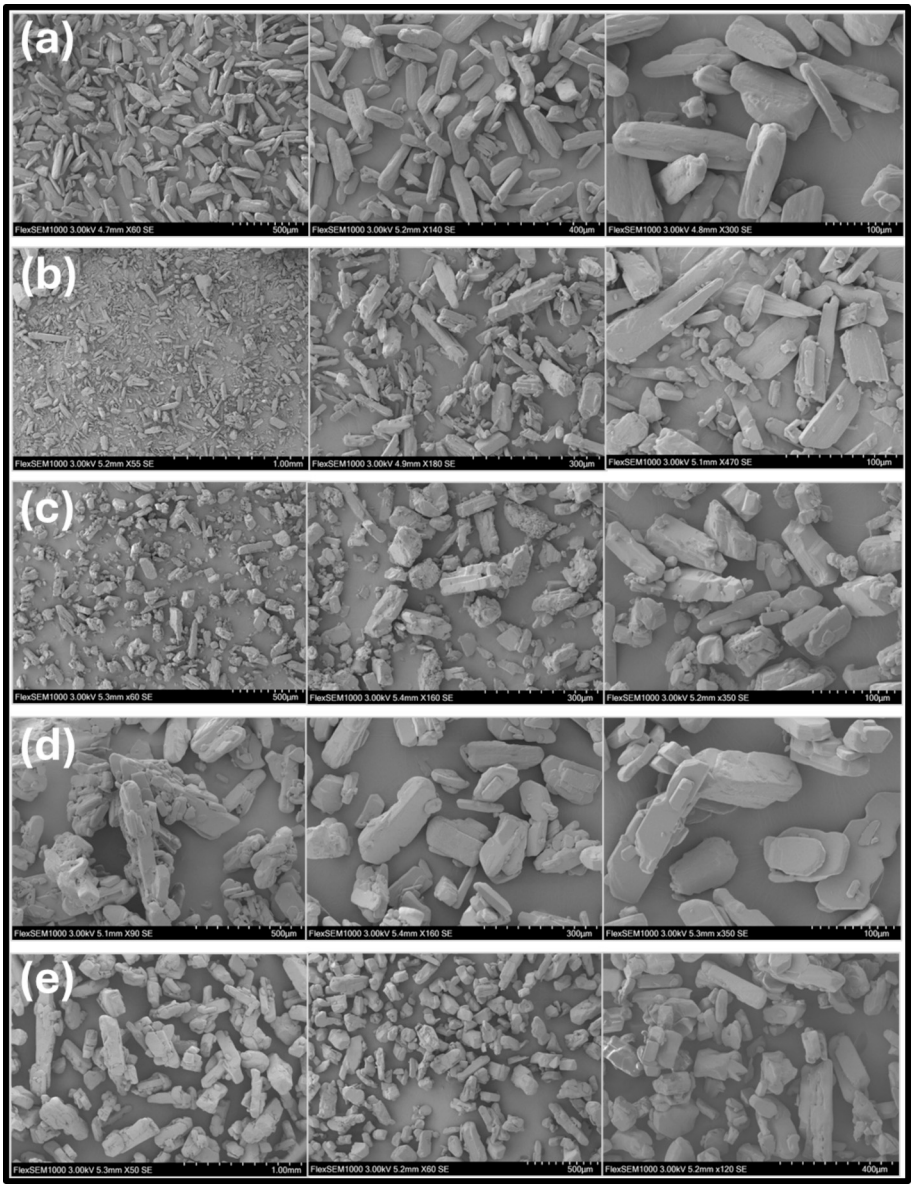

Fig. 2. SEM comparison of recrystallised ibuprofen from different solvents. a) Stock as received b) Hexane c) Acetonitrile *d*) Ethanol e) Methanol.

Table 1
Volume based particle parameters captured using the G3 morphology.

Batch sieve cut	CE Diameter D_{10} (μm)	CE Diameter D_{50} (μm)	CE Diameter D_{90} (μm)	Aspect Ratio D_{10}	Aspect Ratio D_{50}	Aspect Ratio D_{90}	Span	Surface area cm^2/mg
Stock_90–106	62	126	174	0.30	0.43	0.62	0.89	0.57
Stock_75–90	51	96	141	0.28	0.41	0.63	0.94	0.72
Stock_53–63	46	78	107	0.28	0.42	0.66	0.78	0.85
Hex_200–280	35	289	370	0.38	0.66	0.87	1.16	0.63
Hex_100–140	26	64	159	0.30	0.50	0.78	2.06	1.14
Hex_45–100	27	60	107	0.28	0.46	0.73	1.35	1.21
EtOH_200_280	95	256	355	0.42	0.63	0.82	1.01	0.32
EtOH_75–140	88	145	200	0.37	0.54	0.76	0.78	0.45
EtOH_45–75	59	88	116	0.35	0.52	0.76	0.65	0.72
MeCN_90–106	39	107	154	0.39	0.61	0.84	1.08	0.80
MeCN_75–90	38	80	118	0.38	0.60	0.83	1.01	0.93
MeCN_53–63	37	62	81	0.37	0.60	0.83	0.72	1.06
Meth_300–425	221	389	507	0.42	0.61	0.84	0.74	0.19
Meth_140–300	186	310	413	0.40	0.57	0.80	0.73	0.20
Meth_140	86	156	231	0.36	0.55	0.79	0.93	0.44

shift D_{90} marginally above the nominal maximum. For example, Stock_90–106 shows $\Delta_{min} = D_{10} -$ (min aperture) $= -28$ μm and $\Delta_{max} = D_{90} -$ (max aperture) $= +68$ μm. Similarly, Meth_300–425 shows $\Delta_{min} = -79$ μm and $\Delta_{max} = +82$ μm.

In both cases, D_{10} falls substantially below the minimum sieve aperture, indicating fines carryover beneath the nominal cutlikely due to agglomeration, particle orientation, or bridging. Conversely, D_{90} often exceeds the maximum sieve aperture, implying that coarse particles can reorient and pass through interstitial gaps or exploit mesh tolerances.

Elongated, needle-like particles (low aspect ratio, AR) tend to deviate further from nominal sieve bounds. For example, Stock_90–106 (AR = 0.43) shows $\Delta_{min} = D_{10} -$ (min aperture) $= -28$ μm and $\Delta_{max} = D_{90} -$ (max aperture) $= +68$ μm. By contrast, more rounded particles such as EtOH_45–75 (AR = 0.52) exhibit smaller offsets: $\Delta_{min} = D_{10} -$ (min aperture) $= +14$ μm (min = 45 μm; $D_{10} = 59$ μm) and $\Delta_{max} = D_{90} -$ (max aperture) $= +41$ μm (max = 75 μm; $D_{90} = 116$ μm). Thus, lower AR generally correlates with larger departures both below and above the sieve-aperture limits.

These discrepancies arise because the G3 method determines particle size from the projected area, converting it to an equivalent circular diameter, whereas sieve analysis depends on the probability that a particle will adopt a pass-through orientation relative to a fixed aperture. In short, G3 yields an orientation-agnostic equivalent diameter, while sieving is intrinsically orientation-dependent.

The span, representing the width of the particle-size distribution, tends to decrease with finer sieve cuts. For example, in the EtOH series the span drops from ≈1.013 for the 200–280 μm cut to 0.650 for the 45–75 μm cut. Differences between solvents are also evident: the Hex fractions show relatively high span values (up to 2.058 for the 100–140 μm cut), indicating a broader size distribution in that range. By contrast, the MeOH fractions are narrower in the coarser cuts (spans ≈0.73–0.74) but broaden for the finest cut (0.929 for Meth_140). These trends likely reflect differences in crystallisation kinetics and agglomeration behaviour arising from solvent–solute interactions (e.g. polarity, supersaturation, and evaporation rate). Larger sieve windows inherently capture a broader range of particle sizes, while solvent properties influence nucleation and growth and thus the uniformity of particle formation.

The aspect ratio at D_{50} provides an index of median particle shape, with lower values indicating more elongated particles. In the Stock series, the D_{50} aspect ratio is relatively constant (≈0.42) across sieve cuts. This consistency likely reflects that the Stock ibuprofen is a commercial-grade material manufactured to tight specifications with a narrow size distribution, often undergoing post-recrystallisation processing to ensure uniformity and tabletability. In contrast, the Hex series shows a higher aspect ratio in the coarser fraction (0.659 for Hex_200–280) that declines to ≈0.461 in the finest fraction (Hex_45–100). EtOH and MeOH display a similar downward trend, indicating that larger, coarser particles tend to be more circular (higher aspect ratios), whereas finer particles are more elongated or irregular. The greater variability and lack of consistent aspect ratios in these batches likely stem from lab-scale, small-batch recrystallisation, which affords less control over supersaturation, cooling, and mixing histories; combined with the absence of post-recrystallisation conditioning, this leads to broader and less uniform particle-shape distributions. Overall, as solvent polarity increases, particle morphology shifts from elongated, needle-like forms to more rectangular, prism-like crystals. This trend is widely reported in the crystallisation literature on ibuprofen, linking solvent choice to crystal habit, surface properties and downstream powder behaviour. [54,55,50,53]. Differences across solvents likely arise from their influence on crystal-growth dynamics. Specifically, interactions between solvent molecules and the functional groups exposed on particular crystal faces (facets). Crystal morphology is governed by the relative growth rates of these faces; changes in habit reflect shifts in the proportions of expressed faces. For ibuprofen, the dominant faces are (100), (011), and (002): the (100) face is largely nonpolar, presenting aliphatic chains, whereas (011) and (002) are polar, exposing carboxylic acid groups. Solvent–solute interactions (e.g. polarity and hydrogen bonding) modulate surface attachment and dissolution kinetics, thereby altering relative face growth rates [54,56]. As a result, different faces are stabilized or expressed to varying extents, producing the observed variations in crystal morphology.

Across all samples, aspect ratio increases from D_{10} to D_{90}. For example, in Stock_90–106 the aspect ratio progresses from 0.3009 (D_{10}) to 0.4298 (D_{50}) and 0.621 (D_{90}). This indicates that the smallest particles (D_{10}) are more elongated, whereas the largest particles (D_{90}) are more equant/rounded. The consistent $D_{10} < D_{50} < D_{90}$ trend across solvent batches suggests that, within any given sieve fraction, smaller particles are less uniform in shape. Coarser particles tend to be more circular (higher aspect ratios), likely because they experience less mechanical attrition and fewer solvent-induced morphological changes, whereas finer particles are more susceptible to breakage or surface erosion, yielding more elongated or irregular shapes (lower aspect ratios).

Videc et al., [57] showed that smaller particles (lower D_{10}) produced under high agitation or elevated supersaturation exhibit slightly reduced roundness. They attributed this to intensified collision forces and the generation of fines, which disrupt particle morphology. Conversely, larger particles preserved their roundness under optimised crystallisation conditions i.e. balanced supersaturation and controlled hydrodynamics. The authors emphasized that abrasive forces (shear and particle–particle impacts), which scale with agitation velocity, promote surface abrasion particularly in small agglomerates, thereby lowering roundness. Taken together, these observations align with the present aspect-ratio trends: recrystallisation-induced variations likely arise from a combination of differential breakage and processing-induced shape modification that varies with particle size. This highlight the tight coupling between process parameters and particle characteristics in crystallisation systems.

As expected, smaller particles yield higher specific surface area. However, absolute surface-area values differ across solvents. Because sieve fractions vary by solvent batch, direct comparisons are appropriate only between the MeCN and Stock samples, which share identical sieve cuts. Comparing matched fractions reveals a clear trend: for each sieve cut, MeCN samples exhibit higher specific surface area than the corresponding Stock sample. For the broadest fraction (90–106 μm), surface area increases from 0.57 to 0.80 cm^2/mg (≈40 %). The mid-size fraction (75–90 μm) increases from 0.72 to 0.93 cm^2/mg (≈29 %) and the finest fraction (53–63 μm) from 0.85 to 1.06 cm^2/mg (≈25 %). These systematic increases in surface area coincide with modest reductions in CE D_{10}, D_{50}, and D_{90} after recrystallisation in MeCN: each percentile diameter shifts downward by roughly 10–30 μm, naturally increasing surface per unit mass. Span values, however, do not change uniformly between batches: Stock spans range from 0.78 to 0.94, whereas MeCN spans range from 0.72 to 1.08. Notably, MeCN_90–106 shows an increased span (1.08), indicating a broader size distribution despite its higher surface area. In contrast, MeCN_53–63 is slightly narrower than Stock_53–63 (0.72 vs 0.78), yet still displays higher surface area. Together, these observations imply that surface morphology (e.g. increased roughness or porosity) contributes alongside modest size reduction to the observed surface-area enhancement.

Aspect-ratio data further support this conclusion: across D_{10}, D_{50}, and D_{90}, MeCN-processed particles are rounder (AR ≈ 0.37–0.61) than the more plate/needle-like Stock particles (AR ≈ 0.28–0.63). Ordinarily, higher aspect ratio (more spherical) particles would reduce specific surface area relative to elongated shapes, yet the opposite is observed. This implies that the surface-area gains in the MeCN batches are driven not solely by shape, but by a combination of finer sizing and altered surface texture e.g. roughened crystal faces or increased micro-porosity induced by the solvent environment during recrystallisation. Differences across solvents are consistent with their effects on nucleation and growth: solvents that favour rapid nucleation tend to produce smaller, more irregular particles with higher specific surface area, whereas conditions that promote slower growth and/or greater agglomeration

yield larger, smoother particles with lower surface area.

3.4. DVS at variable humidity percentage

The Stock ibuprofen was first analysed by DVS. In DVS, the vapour concentration around a sample is systematically varied while the resulting mass change is recorded, yielding adsorption–desorption behaviour under defined conditions. Both organic and water vapour sorption can be studied with real-time partial-pressure control. Here, water vapour was used to track mass changes in Stock samples under isothermal and stepped-RH conditions.

The first DVS experiment was performed at 25 °C on the as-received Stock powder (prior to sieving) using a single RH cycle. Relative humidity was increased in 10 % steps from 0 % to 90 % and then decreased in 10 % steps back to 0 %. At each step, RH was held until mas equilibrium, defined as a mass-change rate (dm/dt) < 0.002 % min^{-1}. This criterion follows common practice in the literature and aligns with user guidelines from two major DVS manufacturers [58], ensuring steady-state conditions before advancing to the next step. A nitrogen carrier gas (≈400 sccm) maintained stable RH and minimised external interference. Real-time mass and RH measurements were used to construct the adsorption/desorption isotherm (Fig. 3), where the red trace denotes mass (mg) and the blue trace the RH profile.

The data show well-defined adsorption and desorption phases, with only a small mass increase despite the large RH excursion. During adsorption (0 to 90 % RH), the sample gained ≈0.047 % of its initial mass, consistent with the hydrophobic nature of ibuprofen and indicative of surface adsorption rather than bulk absorption. Upon desorption (90 to 0 % RH), the mass returned to baseline, closely mirroring the adsorption path. This reversibility suggests weak, physical binding of water with no evidence of hydrate formation or permanent structural change across the RH range tested.

The negligible mass change reflects ibuprofen's intrinsic hydrophobicity, few polar functional groups and a predominantly non-polar aromatic ring [59]. This result agrees with prior reports of minimal moisture uptake even at high RH (e.g. < 0.035 % at RH > 80 %) [37]. Such limited water sorption supports robust powder handling and formulation by reducing moisture-induced degradation, preserving crystallinity and promoting dose uniformity [60].

3.5. DVS at fixed humidity percentage

A second DVS experiment was conducted on the as-received Stock powder (prior to sieving) under isothermal–isohumidity conditions of 50 °C and 50 % RH. Fig. 4 shows the percentage of initial mass remaining versus time (x-axis: time; y-axis: % mass remaining). The data

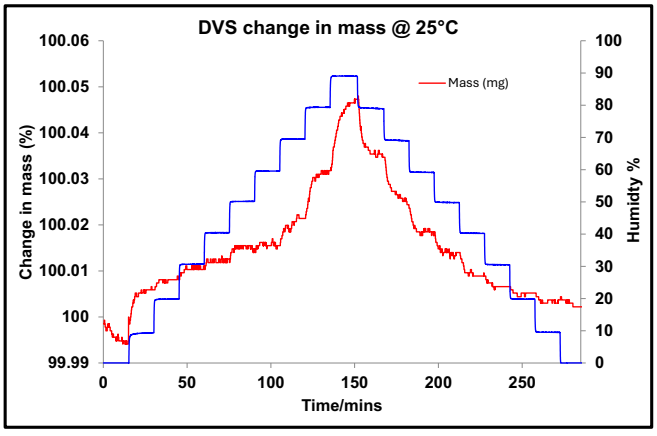

Fig. 3. DVS profiles for stock ibuprofen measured at 25 °C over varying relative humidity levels (%RH).

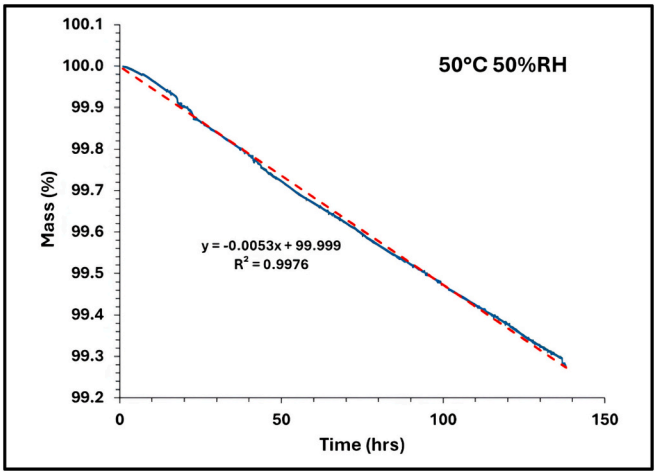

Fig. 4. DVS profile of isothermal conditions of Stock Ibuprofen at constant 50 °C temperature and 50 % humidity.

exhibit an essentially linear decline over 150 h. A linear fit (dotted red line) gives a slope of −0.0053 % h^{-1} with R^2 = 0.9976, indicating uniform mass loss over time (≈0.80 % total over 150 h).

The mass loss observed under fixed 50 °C/50 % RH, but not in the stepped-RH test at 25 °C, is attributed to (i) the much longer measurement window (150 h vs 300 min), which resolves slow processes, and (ii) the higher temperature, which provides sufficient thermal energy for surface molecules to overcome lattice binding and sublimate. At 50 % RH, limited water adsorption offers little hindrance to volatilisation, so sublimation proceeds more readily; lower ambient humidity further facilitates escape of molecules into the vapour phase, accelerating mass loss [61,62]. Consistent with sublimation principles, elevated temperature and modest humidity increase molecular kinetic energy and favour volatilisation [28].

3.6. Sublimation rate

To investigate the sublimation behaviour further, the rate of mass loss for stock as received ibuprofen powder and the four recrystallised batches were tested in TGA at three different temperatures (40 °C, 50 °C, and 60 °C) with near zero RH (constant flow nitrogen), and DVS at constant 50 % RH and temperature levels (40 °C, 50 °C, and 60 °C). Results for all sieve cuts and batches, for both TGA and DVS, are shown in Fig. 5.

The mass-loss rate increases with temperature in both TGA (40, 50, 60 °C; nitrogen, ≈0 % RH) and DVS (50 % RH), reflecting the rise in vapour pressure at elevated temperature and the resulting larger driving force for mass transfer. Accordingly, the addition of thermal energy accelerates sublimation, offering insight into the thermal stability and sublimation kinetics of ibuprofen. The strong temperature dependence is consistent with Arrhenius-type behaviour. At any given temperature, TGA yields higher mass loss than DVS. TGA largely isolates thermal effects by minimising moisture interactions, whereas DVS captures the influence of ambient humidity and thus better represents storage-relevant conditions. This comparison helps discriminate purely thermal contributions from moisture-affected mechanisms, which are discussed later in this section.

DVS data at 40, 50, and 60 °C under a constant 50 % RH indicate that temperature is the dominant driver of mass-loss rate even in humid conditions. For example, for Stock (D_{50} = 77.91 μm), the DVS rate at 60 °C/50 % RH is 62 % lower than the TGA rate at 60 °C/0 % RH. By contrast, increasing temperature from 40 to 60 °C raises the mass-loss rate by 175 % in TGA (0 % RH) and by 172 % in DVS (50 % RH). Table 2 summarises (i) the percent differences in mass-loss rate between TGA (0 % RH) and DVS (50 % RH) at fixed temperatures (40, 50, 60 °C),

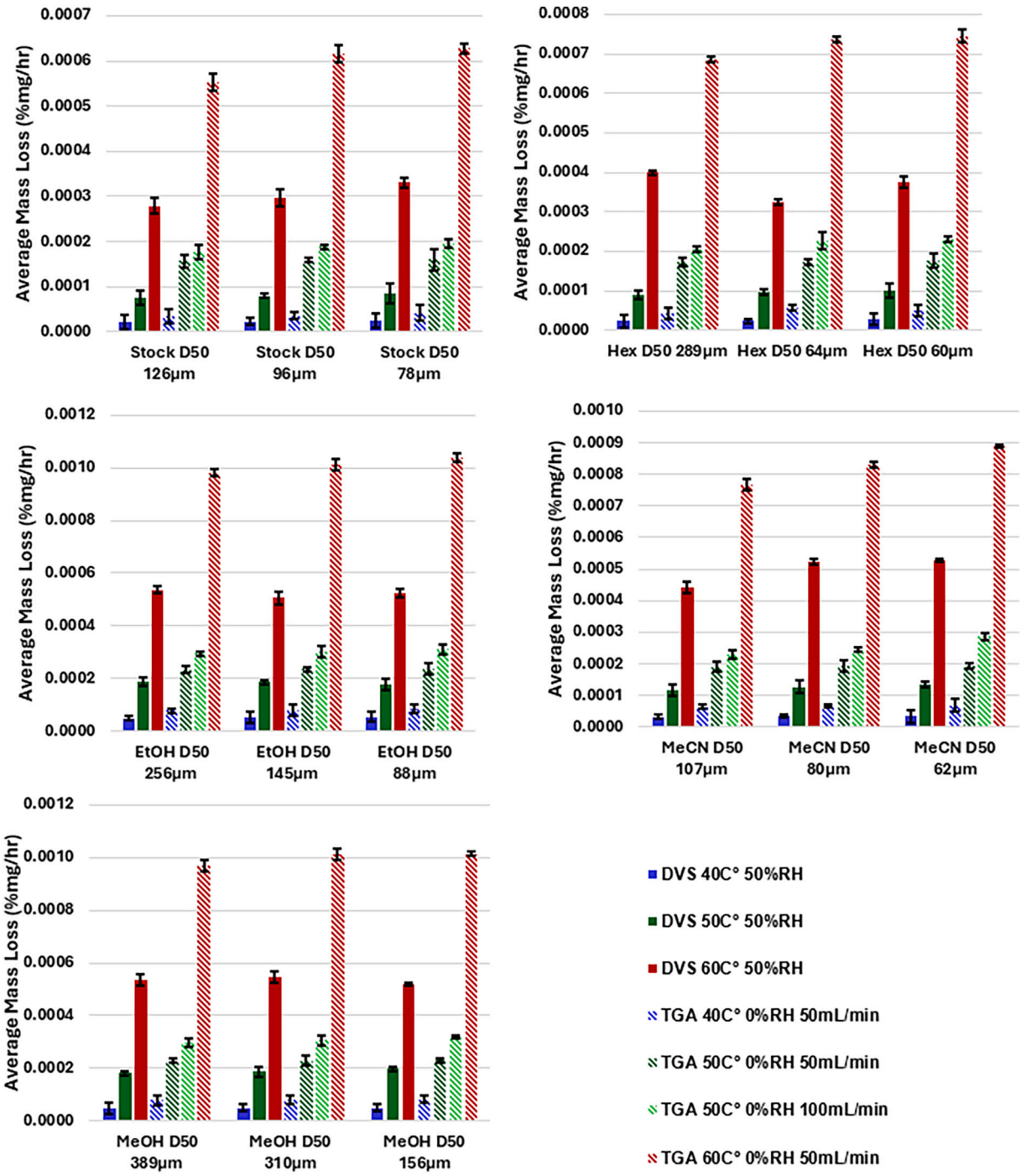

Fig. 5. Average sublimation rates of solvent-recrystallised ibuprofen sieve fractions measured by TGA and DVS at 40 °C, 50 °C, and 60 °C. Error bars represent the standard deviation across three replicate measurements for each sample ($n = 3$).

and (ii) the temperature-induced changes from 40 to 60 °C within each technique. Together, these comparisons highlight humidity sensitivity at fixed temperature and strong thermal sensitivity under both dry and humid conditions.

One explanation for the difference in a dry atmosphere (0 % RH) is that the driving force for sublimation is higher, resulting in faster mass loss. Under a 50 % RH, the ambient moisture partially saturates the vapour phase, thereby reducing the net driving force for mass removal. It is also possible for the moisture in the humid conditions to form a protective barrier onto the particles inhibiting the sublimation process. An example of this is the MeOH recrystallised sample MeOH D_{50} 156 µm displaying a 15 % reduction in mass-loss rate when conditions are changed from TGA 50 °C 0 %RH to DVS 50 °C 50 %RH. The presence of water molecules may stabilise the ibuprofen molecules by forming hydrogen bond interactions with the OH groups at the surface which reduces the mass-loss rates compared to dry conditions. Another explanation is the difference in volume of the sample chamber for both instruments. TGA has a chamber sample volume of 20 mL whereas DVS has chamber with volume of 99.15 mL. The larger DVS chamber volume increases the time required for sublimated ibuprofen molecules to saturate the gas phase delaying the establishment of equilibrium between the solid particles and their vapour. The increased vapour phase residence time in the DVS due to larger chamber volume slows the equilibration in DVS, which diminishes the driving force for sublimation

Table 2
Illustrates the % change in mass-loss rate at 40, 50, and 60 °C when moving from TGA (0 % RH) to DVS (50 % RH). And the % change in TGA-measured rate from 40 °C to 60 °C at 0 % RH and 3- the % change in DVS-measured rate from 40 °C to 60 °C at 50 % RH.

Batch sieve cut	Mass-loss rate % change (TGA 40C° 0 %RH to DVS 40C° 50 %RH)	Mass-loss rate % change (TGA 50C° 0 %RH to DVS 50C° 50 %RH)	Mass-loss rate % change (TGA 60C° 0 %RH to DVS 60C° 50 %RH)	TGA Mass-loss rate % change (40C° to 60C°)	DVS Mass-loss rate % change (40C° to 60C°)	Mass-loss rate % change (flow rate 50 mL to 100 mL @ TGA 50C° 0 %RH)
Stock D_{50} 126 μ	−46.2	−70.4	−66.1	176.5	171.2	11.4
Stock D_{50} 96 μm	−45.4	−66.7	−70.0	178.2	172.0	16.7
Stock D_{50} 78 μm	−52.2	−61.9	−62.0	175.1	172.5	20.1
Hex D_{50} 289 μm	−62.1	−64.5	−52.9	176.3	178.4	17.2
Hex D_{50} 64 μm	−84.5	−55.7	−78.1	171.3	173.3	26.9
Hex D_{50} 60 μm	−56.9	−54.9	−66.0	175.2	172.8	26.5
EtOH D_{50} 256 μm	−44.7	−21.2	−58.6	170.8	166.5	23.2
EtOH D_{50} 145 μm	−42.2	−23.0	−67.0	170.9	162.8	24.8
EtOH D_{50} 88 μm	−41.7	−28.1	−65.9	170.4	162.4	27.6
MeCN D_{50} 106 μm	−66.5	−47.3	−54.1	169.1	172.8	18.6
MeCN D_{50} 80 μm	−61.5	−41.6	−45.2	170.2	174.7	23.8
MeCN D_{50} 62 μm	−66.8	−35.3	−51.0	171.9	176.1	38.4
MeOH D_{50} 389 μm	−49.4	−22.1	−57.8	170.3	167.7	26.2
MeOH D_{50} 310 μm	−48.6	−20.4	−59.7	170.9	167.5	28.9
MeOH D_{50} 156 μm	−47.6	−15.5	−64.8	170.4	164.8	32.6
Average	−54.4	−41.9	−61.3	172.5	170.4	24.2

and thus lowers the net mass-loss rate relative to TGA. In contrast, the much smaller TGA chamber volume permits faster residence time and rapid vapour saturation and more efficient mass transfer. Consequently, the delayed vapour build up in DVS consistently suppresses the thermodynamic impetus for molecules to escape the crystal lattice accounting for the lower mass-loss rates observed across all samples under identical temperature conditions. This distinction highlights the impact of chamber geometry on the kinetics of sublimation processes in TGA and DVS analyses. Although DVS conditions lead to lower overall mass-loss rates compared to TGA (0 % RH), the temperature dependence persists therefore reinforcing the conclusion that the sublimation of ibuprofen is inherently temperature driven regardless of ambient moisture conditions.

Another factor to consider is the effect of gas flow in the system on the rate of ibuprofen mass loss. When comparing the mass-loss rates obtained from TGA data at 50 °C under 50 mL/min vs 100 mL/min flow of nitrogen. The higher flow rate resulted in an average increase of 22.4 % in the mass-loss rate across all samples. Stock D_{50} 126 μm showed the smallest increase of ≈ 11 % where as MeCN D_{50} 62 μm sample exhibited the largest increase of ≈38 %. Table 2 shows the percentage increase for all the samples examined. Increasing the gas flow likely reduces the boundary layer resistance around the particles. This facilitates more rapid removal of the volatile species. Although the increase is modest, it indicates that the sublimation kinetics are at least partly mass transfer controlled.

Analyses across all batches and temperature levels suggest that as the D_{50} decreases (i.e. finer powders) the rate of mass loss is accelerated (Fig. 5). Smaller particle sizes imply a higher surface area-to-volume ratio. This geometric effect enhances the rate at which material is removed by sublimation. Hex sample with a very large D_{50} (289 μm) exhibits much lower mass-loss rate compared to its finer counterparts (D_{50} 64–60 μm). For example, at 40 °C TGA the Hex D_{50} 289 μm sample shows a reduction of 74.7 % and 80.8 % in mass lose rate when compared to the mass-loss rate of the samples Hex D_{50} 64 μm and 60 μm respectively. A similar trend is observed for EtOH sample, as the D_{50} decreases from 256 μm to 88 μm, the TGA 40 °C mass-loss rate increases by 139 %. Both MeCN and MeOH batches show the same trend: mass-loss rate increases as D_{50} decreases, consistent with the higher surface-area-to-mass ratio of finer particles. At comparable D_{50} values, absolute rates for MeCN are modestly higher than for MeOH. This difference likely reflects solvent-dependent crystal habit and surface characteristics (e.g. roughness/porosity and the distribution of polar faces) established during recrystallisation, rather than any EtOH-induced polarity effect.

Because sublimation is largely surface-controlled, particle geometry dominates: coarser particles, with lower surface area per unit mass, naturally exhibit lower absolute mass-loss rates. Normalising the rate by surface area removes this geometric contribution, allowing differences in sublimation kinetics to be attributed to intrinsic material properties or process factors (e.g. the recrystallisation solvent). To explore these effects, the surface-area normalisation should be applied so that non-geometric influences on mass loss can be assessed more directly.

If after normalisation all particles behaved in a “perfectly” surface-controlled manner (with no additional size-dependent geometric effects), one would expect the normalised rates from all the samples to converge to a similar value regardless of particle size. The set of graphs (Fig. 6) displays the rate of mass loss (DVA and TGA) for each sample after correction for size using the calculated surface area of the particles in the samples. As previously mentioned before normalisation, the rates of mass loss increase with decreasing particle size, largely because of the increased surface area available for mass transfer. After normalising for surface area, the rates of mass loss across the different samples sizes became more comparable, suggesting that geometric surface area play primary role in affecting the sublimation rate. As shown in Fig. 6, once mass-loss rates are normalised by surface area, the residual size effect is modest: most samples still show a slight increase in the area-normalised rate with decreasing particle size, but the differences are far smaller than in the unnormalised data. This indicates that the apparent size dependence is largely geometric (surface area–driven), with only a minor residual contribution. The remaining size dependence likely reflects non-geometric factors such as differences in surface chemistry, roughness/porosity and the relative exposure of crystal facets. For example, in the MeCN series at TGA 60 °C, comparing D_{50} = 62 μm vs 107 μm shows a 41.8 % difference in absolute mass-loss rate that shrinks to 14.5 % after

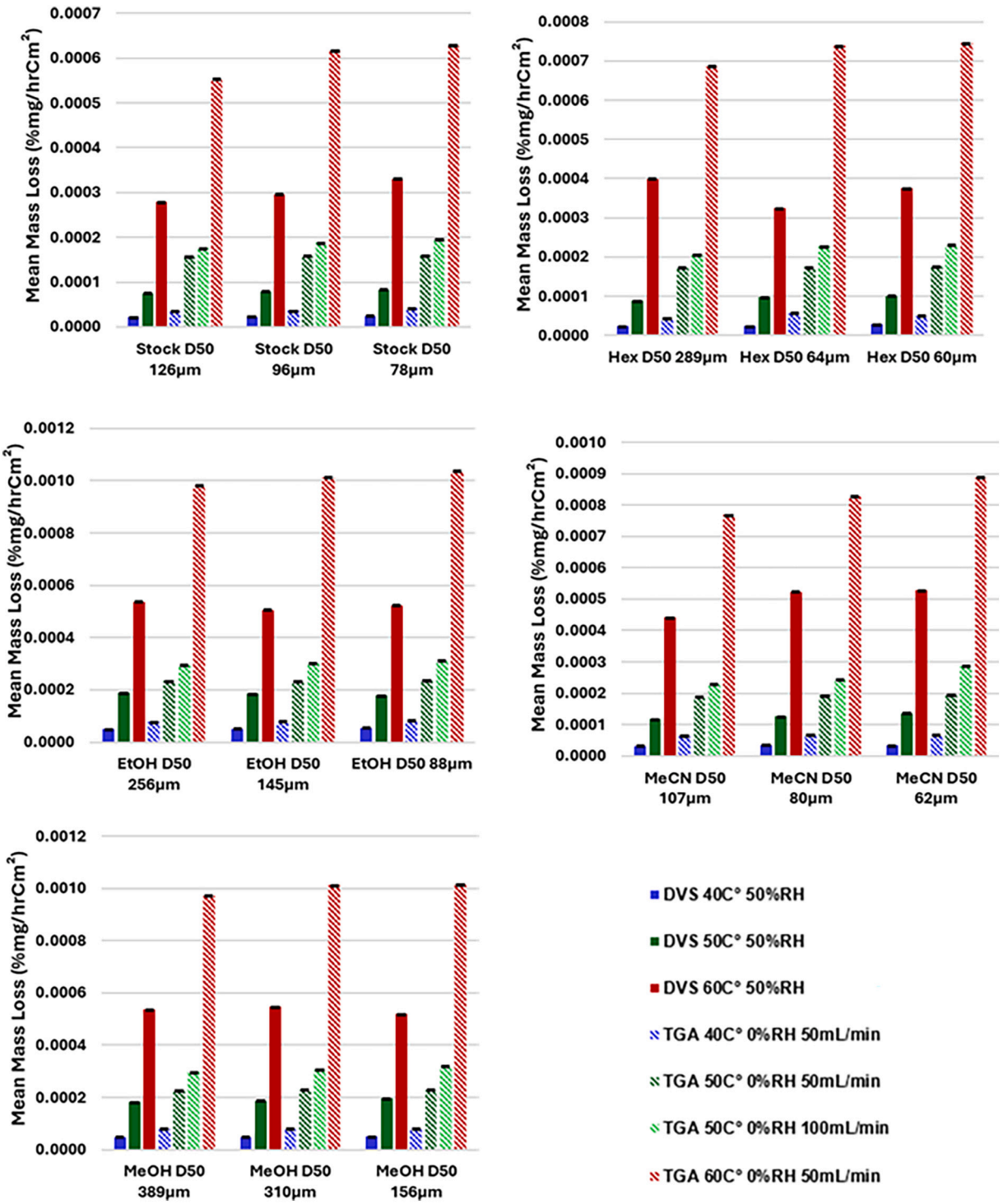

Fig. 6. Surface-area-normalised sublimation rates of solvent-recrystallised ibuprofen sieve fractions measured by TGA and DVS at 40 °C, 50 °C, and 60 °C.

surface-area normalisation. In the Hex series at TGA 40 °C, the D_{50} = 289 µm vs 60 µm comparison drops from 73.9 % (absolute) to 12.8 % (normalised). For EtOH at TGA 60 °C, the difference between D_{50} = 88 µm and 256 µm falls from 80.8 % (absolute) to 5.6 % (normalised). These reductions indicate that the apparent size dependence is dominated by geometry (surface area per unit mass). Residual differences among the finer fractions suggest additional, non-geometric contributors e.g. morphology, surface chemistry/facet exposure or trace residual solvent. In the EtOH series, even though normalised values converge more closely than in Hex, slight discrepancies persist, consistent with solvent history influencing crystal habit and surface functional-group presentation and thereby modulating sublimation kinetics.

As discussed above, surface-area normalisation removes most of the geometric contribution to sublimation. Nevertheless, residual differences remain where smaller particles still show greater mass-loss rates than larger ones, particularly in the Hex and MeCN series implicating surface chemistry and facet exposure. Facet-specific interactions are critical for ibuprofen. Among the dominant faces, the (100) face is largely non-polar, presenting outward-oriented aliphatic chains. This hydrophobic surface inhibits interactions with water and other polar

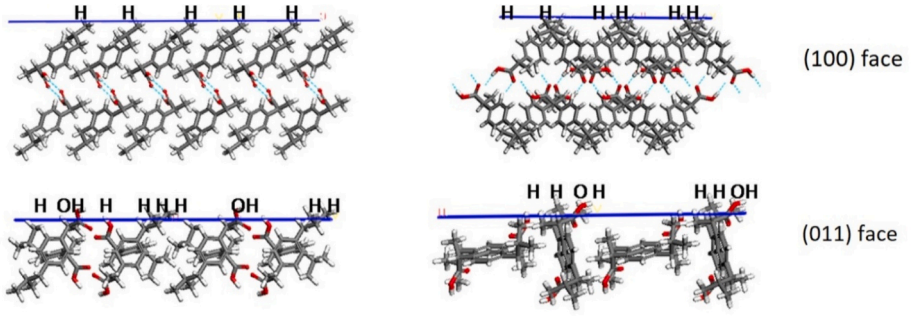

Fig. 7. Molecular packing of ibuprofen on the (100) and (011) facets. Relative to (100), the (011) face shows a more open arrangement and fewer hydrogen-bonding interactions, which is consistent with lower lattice stability.

species; moreover, because the carboxylic acid groups point inward, they form an intra-lattice hydrogen-bond network (Fig. 7) that strengthens the crystal. By contrast, the (011) face is polar, exposing carboxylic acid groups at the surface. Its hydrophilic character promotes interaction with ambient moisture and polar molecules, while the inward-oriented aliphatic chains rely primarily on weaker van der Waals contacts within the lattice. Thus, residual size dependence after normalisation likely reflects shifts in the proportion and accessibility of these faces, with finer fractions presenting more polar, less strongly bound surface area and therefore higher area-normalised mass-loss rates.

The (100):(011) facet-area ratio (reported as "100:011") was calculated for each batch and size fraction. A lower ratio indicates relatively less non-polar (100) surface and a greater fraction of polar (011) surface. This trend helps explain the residual differences in area-normalised mass-loss rates: particles with lower (100):(011) ratios i.e. fewer hydrophobic (100) faces and more hydrophilic, carboxyl-terminated (011) faces exhibit higher mass-loss rates. The pattern is consistent across batches. (See Fig. 8).

In the experimental data, as particle size decreases both the normalised mass-loss rate (after accounting for the effect of surface area) and the (100):(011) ratio decrease (See Table 3). For example, in the Stock batch of particles, the (100):(011) ratio reduces from approximately 0.77 for the D_{50} 126 μm particles to about 0.536 for the D_{50} 78 μm. Similar pattern is seen across all particle sizes and solvents. This indicates that smaller particles are relatively enriched in polar (011) facets. Due to the ibuprofen molecules orientation in the (011) facets more van der Waals interactions will occur within the lattice resulting in weaker crystal facet bonds relative to particles that contain mainly (100) facets. Hence particles with greater amount of (011) facets will have increased rate of mass loss and sublimation as the tendency of ibuprofen molecules to escape the crystal is greater (higher vapour pressure) as a result of increased kinetic energy from elevated temperature environment. Direct surface-specific measurements (e.g. atomic force microscopy) would provide stronger evidence for the proposed facet-dependent sublimation. In future work, we will perform atomic force microscop (AFM) to quantify facet topography, roughness and step density across facets.

Table 3
Ratio of the two principal crystal facets in ibuprofen particles across all samples.

Batch & Particle Size	(100):(011) Ratio
Stock D_{50} 126. μm	0.77
Stock D_{50} 96 μm	0.722
Stock D_{50} 78. μm	0.536
Hex D_{50} 289 μm	0.713
Hex D_{50} 64 μm	0.705
Hex D_{50} 60 μm	0.618
EtOH D_{50} 256 μm	0.896
EtOH D_{50} 145 μm	0.846
EtOH D_{50} 88 μm	0.803
MeCN D_{50} 106 μm	0.678
MeCN D_{50} 80 μm	0.598
MeCN D_{50} 62 μm	0.573
MeOH D_{50} 389 μm	0.927
MeOH D_{50} 310 μm	0.905
MeOH D_{50} 156 μm	0.86

When designing crystallisation processes or optimising manufacturing method it is important to consider not only the particle size (and hence the surface area) but also the surface chemistry. By

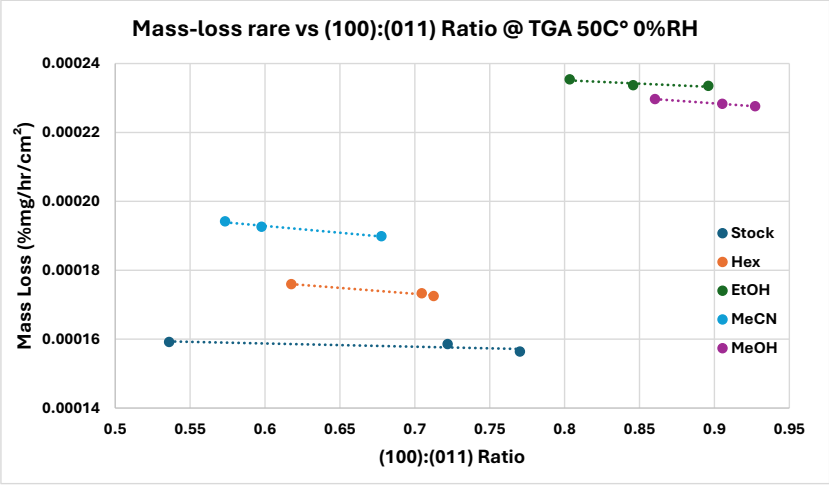

Fig. 8. Relationship between the mass-loss rate measured by TGA at 50 °C and 0 % RH and the change in the ratio of the two dominant ibuprofen crystal facets.

controlling the crystallographic orientation during crystallisation through solvent optimisation (which in turn affects the (100):(011) ratio), one can tailor the sublimation kinetics and hence particle behaviour. For instance, particles with a high (100):(011) ratio is expected to have lower sublimation rate and loss less mass over time during storage, even when surface area is controlled. The combination of high surface area and a surface enriched in polar (011) facets works synergistically to promote rapid mass loss. This insight helps explain why, even after normalisation for surface area, a subtle but consistent differences in mass-loss rates are observed among different batches. As both the physical (surface area) and chemical (facet composition) attributes of the particles must be considered to fully understand the behaviour of ibuprofen and optimise its manufacturing processes.

3.7. Effect of solvent on sublimation rate

To understand the sole influence of solvents on the mass-loss rate and consequently the impact of solvent choice on sublimation behaviour of ibuprofen, the average mass loss of the three particle sieve cuts from each solvent was calculated after normalising for the effect of surface area. Under TGA conditions (0 % RH), polar solvents (EtOHand MeOH) consistently exhibit the highest mass-loss rates across all conditions (temperatures and gas flow rates) (Fig. 9). For example, at 60 °C with 50 mL/min gas flow, EtOH and MeOH display an increase of 51.2 % and 50.1 % in mass-loss rates respectively when compared to stock sample. But when compared to non-polar solvent Hex a rise of 33.2 % and 32.1 % is seen respectively. On the other hand, comparing Hex with the stock sample a moderate increase of 18.8 % in mass-loss rate. Whereas MeCN (semi-polar solvent) consistently produces intermediate mass-loss rates of only 32.1 % greater than the stock sample falling between the results for Hex and those for EtOH or MeOH.

The observed differences can be attributed to the surface characteristics caused by the solvents during recrystallisation. EtOH and MeOH being polar solvents they increase the surface energy of ibuprofen particles. This occurs as more polar functional groups such as COOH are exposed on the surfaces of ibuprofen particles. At the same time the number of hydrogen bonds occurring internally within the crystal lattice decrease and more van der Waals interactions occur between alkyl functional groups. This results in weaker intermolecular interactions and fewer strong intermolecular interactions and thus weakening the overall structure of the crystal and making it easier for molecules to escape the crystal lattice under thermal stress. The opposite occurs for non-polar solvent recrystallised particles where low surface energy occurs due to alky functional groups being exposed on the surface and carboxyl group being internally located causing a series of hydrogen bonds that increases the strength of the crystal lattice.

The standard deviation values for EtOH and MeOH are relatively low (0.000003 and 0.000002 respectively at 40 °C TGA) suggesting consistent behaviour across samples likely due to homogeneous crystal growth with minimised defects and uniform surface modification throughout the particles. In contrast, MeCN produces moderate mass-loss rates with higher variability (standard deviation of 0.000022 at 50 °C TGA). This is due to its semi-polar nature that enables partial polar group exposure combined with the occurrence of rougher surfaces with fine particles attached to the main crystals (Fig. 2). These fine particles exhibit higher sublimation rates before the main crystals start to degrade. Mas loss from this solvent batch likely initiates from the loosely bound fine particles which sublimate rapidly before the main crystals degrade thus introducing variability in mass-loss rates due to inconsistent distribution of these particles. This is confirmed by examining the size distribution of the samples (Table 1). Hex and MeCN have the broadest size distribution than other samples (2–3 times for Hex and 1.2–1.7 times larger for MeCN) suggesting the presence of fine particles which increases the variability in the mass-loss rates. Similarly, Hex also resulted in elevated standard deviations (0.000039 at 60 °C DVS) and MeCN (0.000049 at 60 °C DVS) but with lowest overall sublimation rates (Hex 0.000723 vs MeCN 0.000828 mg/h/cm^2 at 60 °C TGA) likely due to rough surfaces, minimal polar groups exposure and reduced surface energy. This corroborates the hypothesis of heterogeneous surface structures and irregular fine particle attachment leading to variable sublimation behaviour.

The effect of the gas flow rate is evident in TGA data at 50 °C where increasing nitrogen flow from 50 to 100 mL/min elevates the mass-loss rates for all solvents with polar solvents again showing the largest absolute increases (EtOH increased by 25.4 %). The relative ranking of mass-loss rates remains unchanged reinforcing the notion that the solvent effect is robust across variations in experimental conditions. The increase is mass loss occurs because removal of sublimated molecules is enhanced due to faster flow of nitrogen accelerating the kinetic process. Hex and MeCN exhibit smaller increases (Hex increased by 23.8 %)

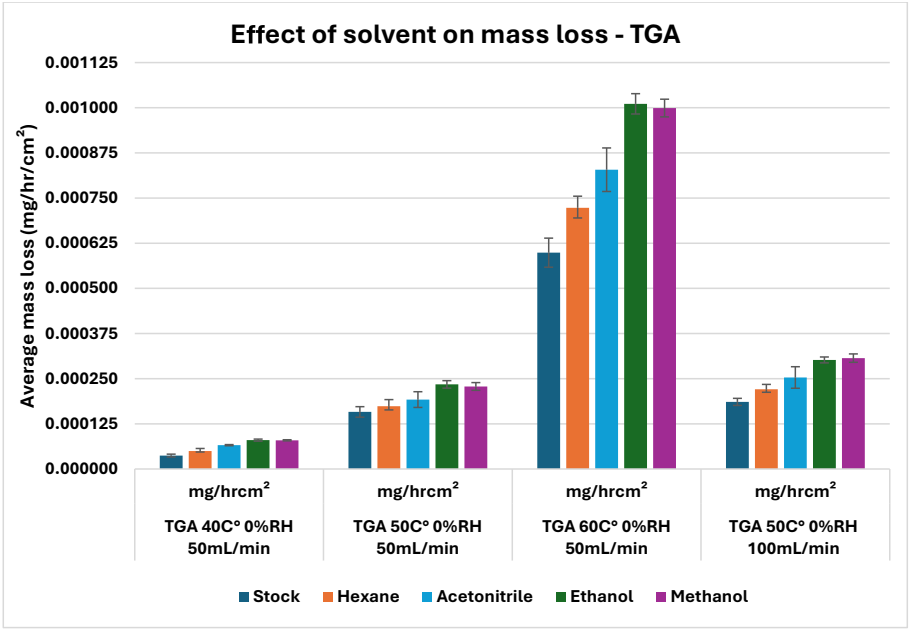

Fig. 9. Surface-area-normalised mean sublimation rates measured by TGA for each recrystallisation solvent.

consistent with their reliance on fine particle sublimation which may be less sensitive to gas flow due to the finite quantity of these particles.

Under DVS conditions with 50 % RH a similar solvent dependent trend is seen but the mass-loss rates are universally lower than as previously discussed. Fig. 10 illustrates again that the mass-loss rates for EtOH and MeOH to be highest across all temperatures ≈2–3 times greater than Hex (60 °C DVS), with MeOH slightly outpacing EtOH at 60 °C (by 2.1 %). MeCN results in an intermediate mass-loss rate while Hex consistently exhibits the lowest rates. The standard deviation values under DVS conditions remain low for EtOH and MeOH reinforcing their consistent behaviour whereas MeCN and Hex show slightly higher variability particularly at elevated temperatures.

To isolate the effect of humidity on solvent polarity during recrystallisation, mass-loss rates for Stock (D_{50} = 96 μm) and MeOH (D_{50} = 310 μm) were measured by DVS at 50 °C under 0 %, 50 %, and 90 % RH. The Stock sample consistently exhibited lower mass-loss rates than the MeOH sample, and both batches showed decreasing rates with increasing RH.

For the Stock sample, the rate of mass loss at 50 % RH was ≈47 % lower than at 0 % RH and a further ≈16 % reduction was observed at 90 % RH. The MeOH sample exhibited a ≈ 39 % decrease when RH increased from 0 % to 50 % RH and an additional ≈24 % decrease at 90 % RH (Table 4). This humidity dependence arises because adsorbed water molecules compete with the sublimating ibuprofen molecules at the particle surface. At higher RH, a quasi-liquid water layer forms, effectively "blocking" sites for mass loss and reducing the net mass flux. Such competitive adsorption phenomena are documented in porous solids and powders undergoing DVS [63].

Across all humidity conditions, the MeOH sample exhibited approximately three-fold higher mass-loss rates than the Stock sample. The primary factor contributing to these observations is treatment with polar solvents such as MeOH alters the surface chemistry of ibuprofen particles by exposing polar functional groups thereby increasing surface polarity. These newly introduced groups promote stronger hydrogen bonding interactions between water molecules and the exposed carboxylic acidmoieties on the drug surface. As a result, the crystal lattice becomes destabilised and the activation energy for sublimation is lowered leading to an enhanced mass-loss rate.

Despite substantial differences in absolute mass-loss rates, both samples exhibit remarkably similar relative declines in sublimation rate with increasing RH thus confirming that a common water layer competition mechanism governing the behaviour. While the magnitude of the rate at any given RH reflects each sample's unique processing history such as differences in surface chemistry, the RH dependence itself appears to be controlled by the physicochemical properties of the adsorbed water layers shared by both materials.

Table 4
Comparison of mass-loss rates for polar versus non-polar ibuprofen batches during DVS at 50 °C, shown as a function of increasing relative humidity.

Batch sieve cut	DVS 50 °C 0 % RH ($\times10^{-6}$ mg/h/cm^2)	DVS 50 °C 50 % RH ($\times10^{-6}$ mg/h/cm^2)	DVS 50 °C 90 % RH ($\times10^{-6}$ mg/h/cm^2)
Stock D_{50} 96 μm	1.71	1.06	0.90
MeOH D_{50} 310 μm	5.26	3.51	2.76

This insight has important ramifications for solvent selection in the commercial crystallisation of ibuprofen. Polar solvents such as EtOH and MeOH tend to yield particles of higher surface energy and correspondingly faster sublimation rates, characteristics that favour rapid dissolution but also promote irreversible interparticle cohesion (caking) during storage. Such caking undermines long-term powder stability and flowability, often requiring energy-intensive milling or sieving steps that introduce defects and broad size distributions thereby compromising product quality and increasing manufacturing costs. By contrast, non-polar solvents (e.g. Hex) and semi-polar solvents (e.g. MeCN) produce particles with lower surface energy and slower mass loss, offering superior storage stability and reduced clumping but at the expense of slower dissolution kinetics an undesirable trade-off for fast-acting analgesics like ibuprofen.

3.8. Enthalpy of sublimation

Sublimation enthalpy is a key macroscopic thermodynamic property that reflects the strength of intermolecular interactions in the solid state [64]. The enthalpy of ibuprofen sublimation was determined using the rate of mass loss under isothermal TGA at 40, 50 and 60 °C temperature profiles.

The Eyring equation (Eq. 2) is derived from transition state theory (activated complex theory), which provides a framework to understand chemical reaction rates. It relates the rate constant (k) of a reaction to the temperature and the activation energy. Transition state theory assumes that for a reaction to occur the reactants must first pass through a high-energy transition state (the activated complex) before forming

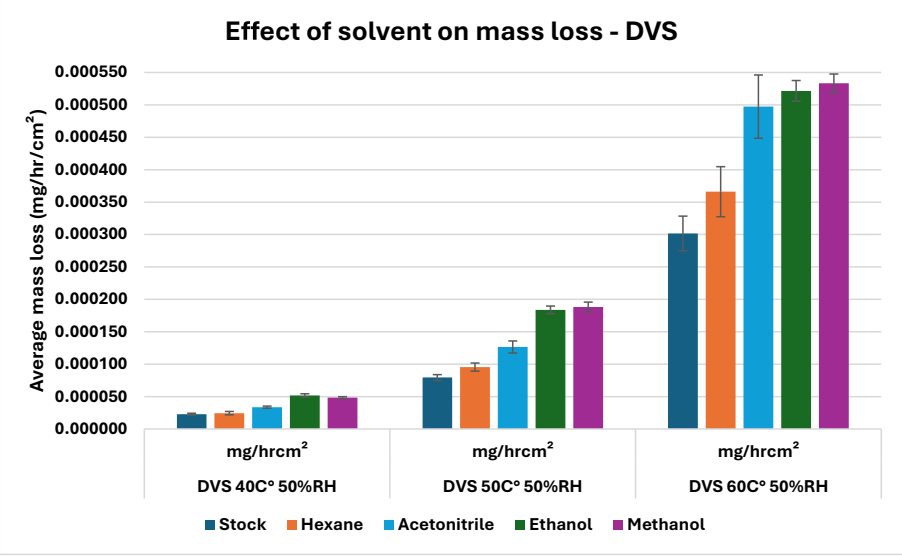

Fig. 10. Surface-area-normalised mean sublimation rates measured by DVS for each recrystallisation solvent.

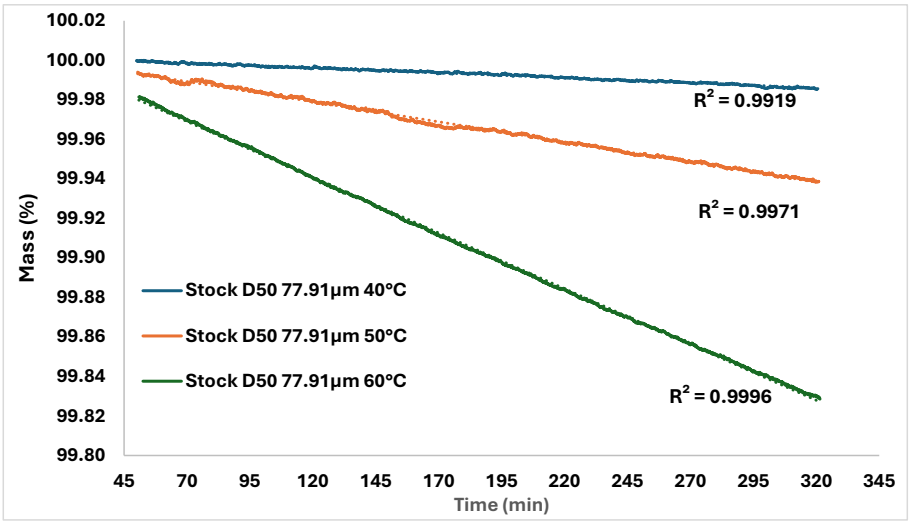

Fig. 11. Isothermal TGA of ibuprofen stock (D50 = 78 µm) showing near-linear mass-loss behaviour at 40–60 °C under a 50 mL/min nitrogen purge.

products [65,66]. The linear nature of the mass loss curves (Fig. 11) implies that the zero-order kinetics was followed over most of the sublimation time. Therefore, the linear form of the Eyring equation can be used to calculate the enthalpy of sublimation for all batches tested due to temperature dependence of sublimation kinetics [67,45]. Where T is the temperature, ΔH the enthalpy of sublimation, k the sublimation rate, ΔS the entropy of sublimation and rate R the molar gas constant.

$$\ln\left(\frac{k}{T}\right) = -\frac{\Delta H}{RT} + \frac{\Delta S}{R} \quad (2)$$

The plot of ln(k/T) versus 1/T gives a straight line with slope from which the enthalpy of sublimation can be derived and an intercept from which the entropy of sublimation is obtained. The Eyring equation was fitted to the data shown in Fig. 12. The sublimation enthalpy (Δ*H*) of ibuprofen was calculated from the slope of a linear regression line and Table 5 shows the results for all batches.A correlation was observed between the enthalpy of sublimation and the TGA mass-loss rate (See Fig. 13.)

The calculated sublimation enthalpy values across the various samples revealed two distinct clusters. Samples prepared using non-polar solvents (Stock and Hex) generally align more closely with the recently reported literature value of 115.7 kJ/mol by Emel'yanenko et al. [68]. Whereby the stock D_{50} 126 µm sample with Δ*H* (114.88 kJ/mol) nearly matching the literature value. However, the stock sample

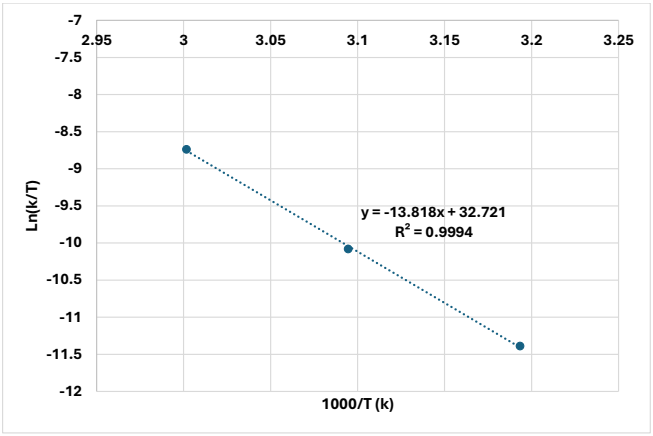

Fig. 12. Eyring plot (ln k/T versus 1000/T) for the sublimation process of stock ibuprofen (D50 = 126 µm), with the linear fit used to estimate sublimation enthalpy.

Table 5
Enthalpy of sublimation for all ibuprofen batches, with regression parameters derived from mass-loss–time curves.

Batch	Enthalpy of sublimation (Δ***H***) kJ/mol	Determination Coefficient (R2)
Stock D_{50} 126 µm	114.89	0.9994
Stock D_{50} 96 µm	121.13	0.9999
Stock D_{50} 78 µm	117.68	0.9988
Hex D_{50} 289 µm	117.11	0.9997
Hex D_{50} 64 µm	108.09	0.9907
Hex D_{50} 60 µm	115.03	0.9970
EtOH D_{50} 256 µm	107.31	0.9910
EtOH D_{50} 145 µm	107.49	0.9988
EtOH D_{50} 88 µm	106.64	0.9914
MeCN D_{50} 106 µm	104.75	0.9988
MeCN D_{50} 80 µm	106.33	0.9985
MeCN D_{50} 62 µm	109.16	0.9989
MeOH D_{50} 389 µm	106.47	0.9986
MeOH D_{50} 310 µm	107.49	0.9985
MeOH D_{50} 156 µm	106.68	0.9985

D_{50} 96 µm with Δ*H* (121.13 kJ/mol) is much closer to the reported value by Ertel et al. [27]. The Hex samples (108.09–117.11 kJ/mol) further reflect the non-polar solvent-specific trend, as the largest sieve cut of the Hex batch (D_{50} 289 µm and Δ*H* 117.11 kJ/mol) approaches the more recent reported literature value. While the Hex D_{50} 64 µm sample (Δ*H* 108.09 kJ/mol) deviates significantly, possibly due to non-uniform crystal packing due to the wide particle size distribution previously discussed.

In contrast, polar solvent-derived batches (EtOH, MeOH and MeCN) consistently yielded lower enthalpies (104.75–109.16 kJ/mol) significantly below the reported literature values for the sublimation of racemate ibuprofen. However, these values are much closer to the sublimation enthalpy of the pure ibuprofen enantiomer with a value of 108.5 kJ/mol as reported by Emel'yanenko et al. [68]. The paper by Maxwell and Chickos, [69] used gas chromatography method to estimate sublimation enthalpies of the racemate and enantiomer and reported the values 128.9 and 122.7 kJ/mol respectively. The high Δ*H*

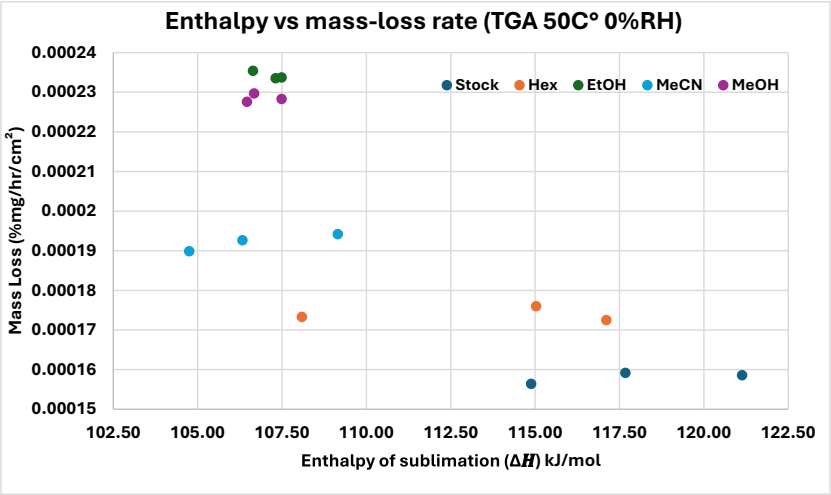

Fig. 13. Correlation between the enthalpy of sublimation and the TGA mass-loss rate determined at 50 °C and 0 % relative humidity.

values reported are due to methodological limitations of chromatography technique, flawed assumptions about enantiomer/racemate behaviour (assumed the vaporisation enthalpy of the racemate and enantiomer are identical) and uncertainties in adjustment of fusion enthalpies. Whereas the paper by Emel'yanenko et al. [68] used direct experimental methods (transpiration and Knudsen effusion) to measure sublimation enthalpy without relying on reference compounds or fusion adjustments. This method is less prone to systematic errors and align closely with theoretical predictions.

As the values of the enthalpy of sublimation are dependent on the experimental methods used for measurement, it is therefore more useful to compare values obtained from the same methods against each other. This study focuses on comparing the enthalpy values derived from polar and non-polar solvent recrystallised ibuprofen batches using isothermal TGA technique. A possible explanation for the reduction in sublimation enthalpies between the polar and non-polar samples is the weaker intermolecular interactions that occur due to the presence of more polar crystal facets. This results in less internal hydrogen bonding within the crystal, which contribute to an overall weaker particles causing the observed differences in sublimation enthalpy.

The MeCN batches exhibit a slight enthalpy increase with decreasing particle size (D_{50} 62 μm: 109.16 kJ/mol vs D_{50} 107 μm: 104.75 kJ/mol), suggesting that with increased surface area causes greater number of facets being exposed on the surfaces further enhancing the effect of facet specific molecular interactions to the overall contribution to crystal integrity. Nevertheless, solvent-driven polar facets dominate as seen in EtOH and MeOH batches where minimal particle-size dependence and seen providing enthalpy of sublimation values near 107 kJ/mol.

The absence of a clear particle-size trend across most solvent groups suggests that solvent effect on facets type and crystal integrity are primary determinants of enthalpy, overshadowing particle size effects. For instance, while smaller particles theoretically exhibit higher surface energy, the influence of solvent in polar batches likely mitigates this contribution. These findings highlight the critical role of crystallisation conditions particularly solvent choice in modulating sublimation thermodynamics.

The Clausius-Clapeyron equation (Eq. 3) is a fundamental equation in thermodynamics that describes the relationship between the enthalpy of sublimation, vapour pressure of a substance and its temperature. It can be derived from the principles of thermodynamics, specifically from the first law of thermodynamics and the concept of phase transitions [70,71].

$$\ln\left(\frac{P_2}{P_1}\right) = \frac{\Delta H}{R}\left(\frac{1}{T_1} - \frac{1}{T_2}\right) \tag{3}$$

Where ΔH the enthalpy of sublimation, R is the universal gas constant and $P_1$and P_2 are the vapour pressures at temperatures $T_1$and T_2, in kelvin respectively.

Existing studies typically determine vapour pressure directly (e.g. by the transpiration method) and then infer sublimation rates (e.g. using Eq. 2). In contrast, we measured the sublimation rate directly and used these data to calculate the enthalpy of sublimation (using Eq. 2). Applying the Clausius–Clapeyron relation, we then estimated the vapour pressure of ibuprofen particles to compare these estimates with literature values. Using our experimentally derived enthalpy of sublimation value (ΔH 114.88 kJ/mol), the Clausius–Clapeyron equation predicts that the vapour pressure at 60 °C is 14.13 times that at 40 ° C. This aligns closely with values reported by Perlovich et al. [28] using the transpiration method, where they reported a vapour pressures of 0.0166 Pa at 40 °C and 0.239 Pa at 60 °C corresponding to a 14.39 fold difference. The close agreement between our estimated vapour pressures and the experimental values reported validates the consistency of our sublimation enthalpy with literature findings, highlighting that measuring the sublimation rate and using these data to estimate vapour pressure is a reliable method. Notably, the minor discrepancy (14.13 vs. 14.39) likely arises from rounding or slight variations in temperature calibration, as highlighted by Emel'yanenko et al. [68] which reconciled prior inconsistencies in ibuprofen's thermodynamic data through combined experimental and quantum-chemical approaches. Future work will incorporate reference standards to make the experimental setup suitable for measuring absolute vapour pressure. Additional measurements will also be acquired to develop an empirical model that more accurately predicts vapour pressure and sublimation behaviour over a wider temperature range.

Overall, the enthalpy of sublimation of ibuprofen is highly sensitive to experimental methodology, complicating direct comparisons across studies. To isolate the influence of solvent choice during crystallisation on the sublimation behaviour of ibuprofen particles below their melting point, normalised sublimation rates (adjusted for surface-area variations) offer a robust analytical framework. This approach circumvents the inherent variability in enthalpy-based comparisons, mitigates confounding methodological factors and enables precise evaluation of how solvent choice affects the physicochemical properties governing sublimation kinetics under sub-melting conditions. By focusing on rate-based analysis, this method provides a clearer, more reliable assessment of solvent-dependent sublimation dynamics.

Collectively, the results identify solvent selection during crystallisation as a practical and effective parameter to control sublimation. By modulating crystal habit and surface chemistry through solvents that favour expression of the (100) facets, it is possible to consistently reduce

mass loss during thermal handling. Targeting a higher (100):(011) facet ratio therefore provides a direct route to limit sublimation-driven mass loss and enhance solid-state stability.

Low-polarity solvents such as Hex, have been shown to preferentially promote growth of the (100) facets, resulting in more stable crystal habits with reduced surface energy. Consequently, crystals formed in such environments exhibit lower mass loss due to sublimation, reduced intra-batch variability and greater reproducibility in downstream processing. The improved control over particle morphology translates into more consistent and efficient batch production, supporting both process robustness and product uniformity.

Furthermore, the same facet-engineering principles can be applied to limit batch-to-batch variation, as even minor shifts in solvent or process conditions can alter the relative exposure of key facets and hence surface chemistry that directly influence sublimation behaviour and powder performance. Selecting solvent systems and process parameters that deliver low-sublimation, facet-stabilized particles enhances surface stability, flowability and compressibility without necessitating additional unit operations, thus improving manufacturing efficiency and reducing production costs.

Practically, we recommend a concise solvent-screening workflow: for each candidate solvent, generate a consistent particle size fraction, quantify facet expression and measure sublimation under representative environmental conditions. Prioritise solvent–process combinations that yield the lowest mass-loss profile and transfer these optimised conditions into scale-up with controls that preserve the desired crystal habits. This solvent-guided crystallisation strategy offers a clear, scalable path to minimise yield loss, tighten batch variability and enhance storage stability.

4. Conclusion

The sublimation behaviour and thermal stability of racemic ibuprofen are shown to be strongly influenced by solvent choice during crystallisation. By systematically varying solvent polarity and environmental conditions, this study establishes a clear link between crystal morphology, surface energetics and sublimation kinetics, offering practical insights for controlling sublimation during pharmaceutical processing and storage.

Key findings from this work are summarised below:

- Solvent polarity dictates morphology and kinetics: Recrystallisation from polar solvents (EtOH, MeOH) yielded more uniform particles with higher-energy surfaces and faster sublimation, while hexane produced irregular, elongated crystals with slower sublimation and superior long-term stability.
- Size and environment effects: Smaller particles sublimed faster (surface-area driven) and humidity suppressed mass loss (DVS at 50 % RH < TGA in dry N_2 at 40–60 °C).
- Structural and chemical integrity: PXRD and FTIR confirmed retained crystallinity and chemical identity across batches; SEM and Morphologi G3 resolved solvent-dependent morphology and size distributions.
- Thermodynamic trends: Enthalpies of sublimation varied with solvent history and followed literature trends; polar-derived batches showed lower values, approaching those of the pure enantiomer. Normalising sublimation rates by surface area enabled solvent-specific effects to be decoupled from particle size.
- Manufacturing relevance: The framework links solvent-controlled morphology and surface energy to measured sublimation under dry and humid conditions, offering a practical solvent-screening approach to minimise sublimation, reduce batch variability and yield loss (e.g. during hot-melt extrusion) and preserve powder attributes critical for tableting and API potency.

Future work will focus on refining predictive control over sublimation through several directions. Absolute vapour pressure calibration will be achieved using reference standards, and the dataset will be expanded by varying pressure, solute concentration, and temperature to enable a more reliable empirical model spanning solvent class and environmental conditions. Additional experiments will include direct measurements of the sublimation front, employing custom-designed cells with optical access and/or in situ imaging approaches to visualise and quantify front propagation in real time. Furthermore, AFM will be applied to correlate facet-level surface properties and roughness with sublimation kinetics and scalability studies will assess long-term stability under industrial crystallisation and storage conditions. Collectively, these efforts will culminate in a validated, predictive framework that translates solvent choice into precise sublimation control, improving yield, quality and consistency in pharmaceutical manufacturing.

CRediT authorship contribution statement

Ameer Alshukri: Writing – review & editing, Writing – original draft, Visualization, Validation, Resources, Project administration, Methodology, Investigation, Funding acquisition, Formal analysis, Data curation, Conceptualization. **Sven L.M. Schroeder:** Writing – review & editing, Validation, Supervision, Resources. **Ana Kwokal:** Supervision, Resources, Conceptualization. **Ali Hassanpour:** Writing – review & editing, Visualization, Supervision, Resources, Formal analysis, Conceptualization.

Declaration of competing interest

The authors declare that they have no known competing financial interests or personal relationships that could have appeared to influence the work reported in this paper.

Data availability

Data will be made available on request.

Acknowledgment

This work was supported by the EPSRC Centre for Doctoral Training in Molecules to Product (Grant Ref. No. EP/S022473/1) as part of a collaborative project with Syngenta Ltd. and Pfizer Ltd. We are especially grateful to Syngenta for facilitating access to their facilities and equipment. All data supporting this study are included in the Results section of this paper or the accompanying electronic supplementary information.

Appendix A. Supplementary data

Supplementary data to this article can be found online at https://doi.org/10.1016/j.powtec.2025.121854.

References

[1] M. de Martino, A. Chiarugi, A. Boner, G. Montini, de' Angelis, G.L., Working towards an appropriate use of ibuprofen in children: an evidence-based appraisal, Drugs 77 (12) (2017) 1295–1311.
[2] A. Mustafa, N. Misailidis, R. Ferreira, D. Petrides, Ibuprofen Continuous Manufacturing – Process Modeling and Techno-Economic Assessment (TEA) Using SuperPro Designer, 2022.
[3] U.V. Shah, V. Karde, C. Ghoroi, J.Y.Y. Heng, Influence of particle properties on powder bulk behaviour and processability, Int. J. Pharm. 518 (1) (2017) 138–154.
[4] M. Chan, *The effect of a source change for an active pharmaceutical ingredient (API) or excipient on the finished drug product.*[online], University of Waterloo, 2016. Available from: https://uwspace.uwaterloo.ca/items/dae2e92c-1141-4f80-9a7f-39a1e611f469.
[5] M. Williams, The Merck index: an encyclopedia of chemicals, drugs, and biologicals. 14th edition. Merck Inc., Whitehouse Station/Rahway, New Jersey, October 2006. Cloth 0-911910-00X. \$125. Pp. 2564, Drug Dev. Res. 67 (11) (2006) 870.
[6] S.B.J. Derry, R.A. Moore, Single dose oral dexibuprofen [S(+)-ibuprofen] for acute postoperative pain in adults, Cochrane Database Syst. Rev. 10 (2013).

[7] G. Leising, R. Resel, F. Stelzer, S. Tasch, A. Lanziner, G. Hantich, Physical aspects of dexibuprofen and racemic ibuprofen, J. Clin. Pharmacol. 36 (12 Suppl) (1996) 3S–6S.
[8] N. Udupa, Characterization of different crystal forms of Iboprofen, Tinidazole and Lorazepan, Drug Dev. Ind. Pharm. 16 (9) (1990) 1591–1596.
[9] V. Labhasetwar, A.K. Dorle, Studies on some crystalline forms of ibuprofen, Drug Dev. Ind. Pharm. 19 (6) (1993) 631–641.
[10] A.J. Romero, C.T. Rhodes, Stereochemical aspects of the molecular pharmaceutics of ibuprofen, J. Pharm. Pharmacol. 45 (4) (1993) 258–262.
[11] A.J. Romero, L. Savastano, C.T. Rhodes, Monitoring crystal modifications in systems containing ibuprofen, Int. J. Pharm. 99 (2) (1993) 125–134.
[12] S.K. Dwivedi, S. Sattari, F. Jamali, A.G. Mitchell, Ibuprofen racemate and enantiomers: phase diagram, solubility and thermodynamic studies, Int. J. Pharm. 87 (1) (1992) 95–104.
[13] S. Lerdkanchanaporn, D. Dollimore, A thermal analysis study of Ibuprofen, J. Therm. Analysis 49 (2) (1997) 879–886.
[14] F. Xu, L.-X. Sun, Z.-C. Tan, J.-G. Liang, R.-L. Li, Thermodynamic study of ibuprofen by adiabatic calorimetry and thermal analysis, Thermochim. Acta 412 (1) (2004) 33–57.
[15] B. Tiţa, A. Fulias, G. Bandur, G. Rusu, D. Tiţa, Thermal stability of ibuprofen. Kinetic study under non-isothermal conditions, Rev. Roum. Chim. 55 (2010) 553–558.
[16] B. Tita, A. Fulias, M. Stefanescu, E. Marian, D. Tiţa, Kinetic study of decomposition of ibuprofen under isothermal conditions, Revista de Chimie -Bucharest- Original Edition-. 62 (2011) 216–221.
[17] D.R. Stull, Vapor pressure of pure substances. Organic and inorganic compounds, Ind. Eng. Chem. 39 (4) (1947) 517–550.
[18] X. Zielenkiewicz, G.L. Perlovich, M. Wszelaka-Rylik, The vapour pressure and the enthalpy of sublimation: determination by inert gas flow method, J. Therm. Anal. Calorim. 57 (1) (1999) 225–234.
[19] G. Sauerbrey, F. Sauerbrey, Use of quartz vibration for weighing thin films on a microbalance, Available from: https://api.semanticscholar.org/CorpusID:222403812, 1959.
[20] R. Speyer, *Thermal analysis of materials* [online], CRC Press, 1993, https://doi.org/10.1201/9781482277425. Available from.
[21] R.G. Cooks, J.H. Beynon, Mass Spectrometry for Chemists and Biochemists, 2nd ed, Cambridge University Press, Cambridge, 1996.
[22] V. Chaurasiya, Numerical modeling of sublimation heat and mass transfer with convective interface and temperature-dependent thermal properties, Int. Communicat. Heat and Mass Transfer. 159 (2024) 108001.
[23] V. Chaurasiya, Numerical simulation of a non-linear sublimation process with temperature-dependent permeability and volumetric heat source: A phase change problem, Comput. Math. Appl. 176 (2024) 55–66.
[24] V. Chaurasiya, A. Jain, J. Singh, Analytical study of a moving boundary problem describing sublimation process of a humid porous body with convective heat and mass transfer, J. Therm. Anal. Calorim. 148 (6) (2023) 2567–2584.
[25] V. Chaurasiya, Rajeev and Kumar, J., Bernstein operational matrix of differentiation to analyze the conductive, convective, and radiative non-linear sublimation model with temperature-dependent internal heat generation, J. Therm. Stresses 47 (11) (2024) 1450–1478.
[26] S.K. Sharma, N. Kumar, N.A. Shah, V. Chaurasiya, Genocchi operational matrix of the differentiation method for phase change process with size-dependent thermal conductivity and mass diffusivity, Chin. J. Phys. 95 (2025) 529–557.
[27] K.D. Ertel, R.A. Heasley, C. Koegel, A. Chakrabarti, J.T. Carstensen, Determination of ibuprofen vapor pressure at temperatures of pharmaceutical interest, J. Pharm. Sci. 79 (6) (1990) 552.
[28] G.L. Perlovich, S.V. Kurkov, L.K. Hansen, A. Bauer-Brandl, Thermodynamics of Sublimation, Crystal Lattice Energies, and Crystal Structures of Racemates and Enantiomers: (+)- and (±)-Ibuprofen, J. Pharm. Sci. 93 (3) (2004) 654–666.
[29] A. Bellec, J.-C. Guillemin, Attempts to explain the self-disproportionation observed in the partial sublimation of enantiomerically enriched carboxylic acids, J. Fluor. Chem. 131 (4) (2010) 545–548.
[30] K. Lin, Y. Wang, Q. Yu, Cocrystallization from ibuprofen–nicotinamide vapor phase mixture in the absence and presence of seeds, J. Cryst. Growth 570 (2021) 126229.
[31] A. Hottot, J. Andrieu, S. Vessot, Sublimation kinetics during freeze-drying of pharmaceutical protein formulation, Drying Technology - DRY TECHNOL. 25 (2007) 753–758.
[32] K. Garbera, K. Woå-Latosi, W. Sawicki, Development of tablets containing solid dispersion of ibuprofen manufactured by hot melt impregnation process, Acta Poloniae Pharmaceutica ñ Drug Research. 76 (2) (2019) 341–354.
[33] P. Mandati, D. Nyavanandi, S. Narala, A. Alzahrani, S.K. Vemula, M.A. Repka, A comparative assessment of Cocrystal and amorphous solid dispersion Printlets developed by hot melt extrusion paired fused deposition modeling for dissolution enhancement and stability of ibuprofen, AAPS PharmSciTech 24 (7) (2023) 203.
[34] L.J. Jallo, C. Ghoroi, L. Gurumurthy, U. Patel, R.N. Davé, Improvement of flow and bulk density of pharmaceutical powders using surface modification, Int. J. Pharm. 423 (2) (2012) 213–225.
[35] M. Nachajski, A. Bazela, M. Zarzycka, A. Broszczyk, A. Kolba, M. Kolodziejczyk, Effect of API on powder Flowability, direct compression and properties of orally disintegrating tablets: A Preformulation study, Indian J. Pharm. Sci. 81 (2019).
[36] H. Matoba, T. Yoshikawa, T. Makino, Pharmaceutical preparation containing sublimable component, Available from, https://patents.google.com/patent/JP2003183181A/en, 2001.
[37] A. Balk, J. Wiest, T. Widmer, B. Galli, U. Holzgrabe, L. Meinel, Transformation of acidic poorly water soluble drugs into ionic liquids, Eur. J. Pharm. Biopharm. 94 (2015) 73–82.
[38] N. Christakis, J. Wang, M.K. Patel, M.S.A. Bradley, M.C. Leaper, M. Cross, Aggregation and caking processes of granular materials: continuum model and numerical simulation with application to sugar, Adv. Powder Technol. 17 (5) (2006) 543–565.
[39] K. Danjo, H. Kato, A. Otsuka, T. Wakimoto, Influence of moisture adsorption of volume shrinkage and Diametral tensile strength of sucrose tablets, Chem. Pharm. Bull. 41 (12) (1993) 2147–2150.
[40] C. Kunz, H. Gieseler, Merits and limitations of dynamic vapor sorption studies on the morphology and physicochemical state of freeze-dried products, J. Pharm. Sci. 107 (8) (2018) 2179–2191.
[41] W. Gückel, R. Kästel, T. Kröhl, A. Parg, Methods for determining the vapour pressure of active ingredients used in crop protection. Part IV. An improved thermogravimetric determination based on evaporation rate, Pestic. Sci. 45 (1) (1995) 27–31.
[42] K. Chatterjee, A. Hazra, D. Dollimore, K.S. Alexander, Estimating vapor pressure curves by thermogravimetry: a rapid and convenient method for characterization of pharmaceuticals, European J. Pharmaceut. Biopharmaceutics 54 (2) (2002) 171–180.
[43] J.P. Elder, Sublimation measurements of pharmaceutical compounds by isothermal thermogravivletry, J. Therm. Anal. 49 (2) (1997) 897–905.
[44] G.-Y. Gao, S.-Y. Lin, Thermodynamic investigations of nitroxoline sublimation by simultaneous DSC-FTIR method and isothermal TG analysis, J. Pharm. Sci. 99 (1) (2010) 255–261.
[45] M. Xie, T.M. Ziemba, M.B. Maurin, Sublimation characterization and vapor pressure estimation of an HIV nonnucleoside reverse transcriptase inhibitor using thermogravimetric analysis, AAPS PharmSciTech 4 (2) (2003) E23.
[46] V. Ruz, M.M. González, D. Winant, Z. Rodríguez, G. den Mooter, Characterization of the sublimation and vapor pressure of 2-(2-Nitrovinyl) furan (G-0) using thermogravimetric analysis: effects of complexation with Cyclodextrins, Molecules 20 (8) (2015) 15175–15191.
[47] B. Koroglu, A.K. Burnham, I. Mashiana, A. Racoveanu, C. Arose, J.C. Crowhurst, J. G. Reynolds, Comparative analysis of sublimation and thermal decomposition of TATB, Propellants, Explos., Pyrotech. 49 (2) (2024) e202300124.
[48] S. Sheokand, S.R. Modi, A.K. Bansal, Dynamic vapor sorption as a tool for characterization and quantification of amorphous content in predominantly crystalline materials, J. Pharm. Sci. 103 (11) (2014) 3364–3376.
[49] G.M. Khan, Z. Jiabi, Preparation, characterization, and evaluation of physicochemical properties of different crystalline forms of ibuprofen, Drug Dev. Ind. Pharm. 24 (5) (1998) 463–471.
[50] N. Rasenack, B.W. Müller, Properties of ibuprofen crystallized under various conditions: A comparative study, Drug Dev. Ind. Pharm. 28 (9) (2002) 1077–1089.
[51] Yanxiang Li, F. Yao, C. Shang, F. Ren, J. Zhang, Yanan Li, G. Yang, R. Lin, W. Wang, Preparation, characterization and in vivo evaluation of pharmacological activity of different crystal forms of ibuprofen, Pak. J. Pharm. Sci. 32 (5) (2019) 2139–2147.
[52] M. Maghsoodi, Role of solvents in improvement of dissolution rate of drugs: crystal habit and crystal agglomeration, Adv. Pharmaceuti. Bulletin. 5 (1) (2015) 13–18.
[53] M.H. Shariare, N. Blagden, M. de Matas, F.J.J. Leusen, P. York, Influence of solvent on the morphology and subsequent comminution of ibuprofen crystals by air jet milling, J. Pharm. Sci. 101 (3) (2012) 1108–1119.
[54] H.A. Garekani, F. Sadeghi, A. Badiee, S.A. Mostafa, D.A.R. Rajabi-Siahboomi, A. R. Rajabi-Siahboomi, Crystal habit modifications of ibuprofen and their Physicomechanical characteristics, Drug Dev. Ind. Pharm. 27 (8) (2001) 803–809.
[55] D. Hooper, F.C. Clarke, R. Docherty, J.C. Mitchell, M.J. Snowden, Effects of crystal habit on the sticking propensity of ibuprofen—A case study, Int. J. Pharm. 531 (1) (2017) 266–275.
[56] T.T.H. Nguyen, R.B. Hammond, K.J. Roberts, I. Marziano, G. Nichols, Precision measurement of the growth rate and mechanism of ibuprofen {001} and {011} as a function of crystallization environment, CrystEngComm 16 (21) (2014) 4568–4586.
[57] D. Videc, O. Planinšek, D. Lamešić, Design of Experiments for optimization of the lactose spherical crystallization process, J. Pharm. Sci. 109 (9) (2020) 2774–2786.
[58] S.V. Glass, C.R. Boardman, E.E. Thybring, S.L. Zelinka, Quantifying and reducing errors in equilibrium moisture content measurements with dynamic vapor sorption (DVS) experiments, Wood Sci. Technol. 52 (4) (2018) 909–927.
[59] A.S. Kashnik, O.Y. Selyutina, D.S. Baranov, N.E. Polyakov, S.A. Dzuba, Localization of the ibuprofen molecule in model lipid membranes revealed by spin-label-enhanced NMR relaxation, *Biochimica et Biophysica Acta (BBA)* - Biomembranes 1865 (8) (2023) 184215.
[60] L.H. Ng, J.K.U. Ling, K. Hadinoto, Formulation strategies to improve the stability and handling of Oral solid dosage forms of highly hygroscopic pharmaceuticals and nutraceuticals, Pharmaceutics 14 (10) (2022).
[61] M.R. Dhondale, P. Thakor, A.G. Nambiar, M. Singh, A.K. Agrawal, N.R. Shastri, D. Kumar, Co-crystallization approach to enhance the stability of moisture-sensitive drugs, Pharmaceutics 15 (1) (2023).
[62] D.-J. Lee, S. Lee, I.W. Kim, Effects of humidity and surfaces on the melt crystallization of ibuprofen, Int. J. Mol. Sci. 13 (8) (2012) 10296–10304.
[63] S. Brunauer, P.H. Emmett, E. Teller, Adsorption of gases in multimolecular layers, J. Am. Chem. Soc. 60 (2) (1938) 309–319.
[64] A. Gavezzotti, G. Filippini, Geometry of the Intermolecular X-H.cntdot..cntdot.. cntdot.Y (X, Y = N, O) Hydrogen Bond and the Calibration of Empirical Hydrogen-Bond Potentials, J. Phys. Chem. 98 (18) (1994) 4831–4837.
[65] H. Eyring, The activated complex in chemical reactions, J. Chem. Phys. 3 (2) (1935) 107–115.
[66] G. Lente, I. Fábián, A.J. Poë, A common misconception about the Eyring equation, New J. Chem. 29 (6) (2005) 759–760.

[67] V.V. Krongauz, M.T.K. Ling, L. Woo, U. Purohit, Kinetics of dihydro-dibenz[b,f] azepine derivatives sublimation, Thermochim. Acta 457 (1) (2007) 35–40.
[68] V.N. Emel'yanenko, K.V. Zherikova, S.P. Verevkin, Quantum chemistry and pharmacy: diagnostic check of the thermochemistry of ibuprofen, ChemPhysChem 25 (11) (2024) e202400066.
[69] R. Maxwell, J. Chickos, An examination of the thermodynamics of fusion, vaporization, and sublimation of ibuprofen and naproxen by correlation gas chromatography, J. Pharm. Sci. 101 (2) (2012) 805–814.
[70] O.L.I. Brown, The Clausius-Clapeyron equation, J. Chem. Educ. 28 (8) (1951) 428.
[71] M. Novaković, N. Ninić, M. Stefanović, A derivation of the Clausius-Clapeyron equation, J. Eng. Phys. 13 (1) (1967) 65–66.